A PRACTICAL APPROACH TO HELICOPTER INTERNAL NOISE PREDICTION

Larry S. Levine and Jon J. DeFelice
Sikorsky Aircraft Division
United Technologies Corporation

SUMMARY

A practical and well correlated procedure for predicting helicopter internal noise is presented. The development of the method was supported by NASA Contract NAS1-14446. It accounts for the propagation of noise along multiple paths on an octave-by-octave basis. The method is sufficiently general to be applicable to conventional helicopters as well as other aircraft types, when the appropriate structural geometry, noise source strengths, and material acoustic properties are defined. A guide is provided for the prediction of various helicopter noise sources over a wide range of horsepowers for use when measured data are not available.

The method is applied to the prediction of the interior levels of the NASA/Sikorsky Civil Helicopter Research Aircraft (CHRA), both with and without soundproofing installed. Correlation with measured levels was very good. Speech Interference Level (SIL) was predicted within 1.5 dB at all conditions. A sample problem is also shown illustrating the use of the procedure. This example calculates the engine casing noise observed in the passenger cabin of the CHRA.

INTRODUCTION

Design efficiency has become an increasingly important characteristic in the helicopter industry as manufacturers strive to improve aircraft performance and operators strive to hold operating costs down. As cabin internal noise requirements become more stringent for increased passenger comfort, soundproofing weight becomes an important issue. A designer needs to know the acoustic environment in a bare aircraft cabin to be able to define an effective soundproofing configuration. It would be a waste of valuable aircraft weight-empty to carry many pounds of soundproofing in areas where they are not needed. But it would also be a serious error if an interior failed to meet the design requirement because not enough soundproofing was used. What is needed is a practical, internal noise prediction method that can provide the distribution and spectral content of the cabin noise signature. The goal is to substitute an analytic evaluation of an interior configuration into the noise model to determine the most efficient placement of treatment weight.

There are many challenges in attempting to formulate and predict helicopter internal noise. The noise observed in a helicopter cabin is produced by several, widely varying source types. For example, rotor noise is generated by the aerodynamic forces of lift and drag. Trans-

mission noise is generated by the mechanical forces transmitted in gear tooth contact. Further complicating the formulation, a given source's noise may be propagated via different means: airborne, structure-borne, or both.

The noise sources that, in general, make a significant contribution to cabin levels are the main transmission, engines, rotors, and boundary layer. Transmission noise is composed of discrete tones at gear clash frequencies and their harmonics and is propagated as both airborne and structure-borne noise. It dominates cabin noise for several reasons. First, the transmission is coupled to the lightly damped airframe which acts as an efficient radiator. Second, primary clash frequencies are high and often fall within the ear's range of peak sensitivity: 500-2000 Hz. Finally, discrete tones are more annoying than broadband noise of the same level. Engine noise is broadband, peaking at 250-500 Hz, except for the compressor shaft rotational and inlet vane passage tones. Its propagation is both airborne and structure-borne and it contributes to the cabin noise spectrum in practically every octave. Rotor noise harmonics are found at the lowest octaves. Their propagation is airborne, but because soundproofing is not very effective at these frequencies, rotor harmonics are difficult to keep out of the cabin. Boundary layer noise is broadband and high in frequency. For this reason it is relatively easy to treat.

An internal noise prediction method must, therefore, be many-faceted. It must integrate ideas from such diverse areas as aerodynamic and structure-borne noise, radiation and propagation effects, material transmission loss and absorption, and rotor, engine, and gear noise source strength prediction. Even though the method must represent a complex physical system, it must also be simple enough to apply within realistic constraints of time and effort. Ideally, it should be sufficiently flexible to be useful in preliminary design as well as in the detail design stage with specific (possible measured) data.

The method discussed in this paper has those capabilities. While a more detailed development and exercise of this method is presented in Reference 1, this paper will serve as a guide to its development and use. The user can assemble the noise model in whatever detail desired. When specific test data is not available for individual noise sources, the generalized prediction methods will provide a reasonable guide. These methods predict rotor, engine, gear, and boundary layer noise source strengths over a wide range of helicopter operating parameters. A means of estimating panel transmission loss based on the barrier's mass, stiffness, and physical dimensions is also included to supplement the user's data base.

The approach of the method is to follow the propagation of each noise source to the observer's location. This may occur via more than one path so each must be dealt with separately. The properties of all intervening barriers and cavities are considered and applied to the sound transmitted through each. This allows one to account for the room acoustics and to show the relative importance of the direct radiated

versus the reverberant fields. The frequency breakdown uses the nine preferred octave bands from 31.5 Hz to 8000 Hz (Reference 2). Most aircraft noise specifications are in octave format. Of prime importance are the three SIL or Speech Interference Level octaves: 500, 1000, and 2000 Hz. These frequencies tend to govern an observer's judgment of a noise environment. Not only is human hearing most acute in this range, but the voice also appears primarily within these three octaves.

The method considers two forms of sound propagation, airborne and structure-borne. Conventional room acoustics is used to represent airborne propagation. For the frequencies and cabin dimensions involved, this approach is reasonable. While cabin standing waves cannot be predicted with this technique, it is assumed that noise measurements are spacially averaged. Only at the lower frequencies, where wavelength and cabin dimensions are of the same order, do the assumptions begin to break down. The propagation and radiation of structure-borne noise is a difficult process to analyze in an exact form. So many unknowns exist in describing the properties (mass, stiffness, and damping) of complex structures that a very simplified approach has to be employed to obtain a workable solution. Some gross assumptions are made concerning the blockage of structure-borne noise at turns, structural breaks, and at heavy frames. These assumptions serve to define the extent and shape of the radiating areas. Skin panels and frames are assumed to radiate uniformly within the areas bounded by structural breaks and equally well at all frequencies. While this is not entirely accurate, present knowledge of the subject is insufficient to permit a more specific analysis. It will remain for further work in the areas of structural impedance and radiation efficiency to formulate an exact solution of the program for arbitrary structures.

SYMBOLS

A_b	rotor total blade area, ft^2
C, C_0, C_1,...	directivity/distance factor
C_{avg}	average directivity/distance factor
c	speed of sound (sea level std), 340 m/sec (1116 ft/sec); blade chord, ft
f_s	rotor broadband noise peak frequency, Hertz
f_o	boundary layer peak frequency
h	projected blade thickness, ft
I, I_{obs}	acoustic intensity, watts/m^2
I_o	reference intensity, 10^{-13} watts/m^2

L	radiating surface dimension, ft
m	harmonic number
N	number of cavities
q	dynamic pressure
$R, R_0, R_1, \ldots$	room constant; distance to observer, ft
r_1	near-field distance
r_2	far-field distance
S_T	total area
S_s	source area
$S, S_0, S_1, \ldots$	barrier area
T	thrust, pounds
t	blade thickness, ft
U_∞	free stream velocity
V_t	rotor tip speed, ft/sec
W, W_i	acoustic power, watts
W_T	total acoustic power, watts
X	distance from leading edge
α	absorption coefficient
$\bar{\alpha}$	average room absorption coefficient
Δ	non-dimensional fluctuating pressure levels
δ	boundary layer momentum thickness
δ^*	boundary layer displacement thickness
ε	% leakage
θ	blade linear equivalent twist; degrees
ρ, ρ_i	density of air, intensity ratio
Σ	sum

σ_i	radiating surface area ratio
τ	transmission coefficient
τ_{eff}	effective transmission coefficient
ω_i	radiating surface power ratio

CONVERSION FACTORS

To convert from	To	Multiply by
ft	m	0.3048
ft^2	m^2	0.0929
horsepower	kW	0.7457
lbm	kg	0.4536
lbf	N	4.448
lbf/ft^2	N/m^2	47.88
$slugs/ft^3$	kg/m^3	515.4

FORMULATION OF THE MODEL

Approach

There are two types of acoustic processes that must be expressed mathematically to predict the internal noise environment. They include the airborne propagation of sound through several cavities and structure-borne propagation over large radiating surfaces, shown in Figure 1. These two propagation modes are the paths by which sound energy reaches the cabin.

It is convenient to break the cabin down into elementary radiating surfaces. The directivity characteristics of these simple radiators determine the direct sound field for a given observer position. The standard equations of room acoustics are used to establish the reverberant field. The two fields are combined to form the complete internal noise environment.

Propagation and Radiation Formulas

Consider an arbitrary surface of some area S to be radiating noise (Figure 2). The total energy emitted by the plate is W (watts). The sound power level (PWL) of this radiating plate relative to a standard source radiating 10^{-12} watts (W_0) is

$$(1) \quad PWL = 10 \log W/(W_0)$$

The intensity I (watts/m^2) on the surface of this plate (outgoing energy per unit area) is related to the plate's area, S. Since

$$W = I \cdot S \qquad \text{or} \qquad I = W/S$$

then the Intensity Level (IL) is

$$IL = 10 \text{ Log } \frac{W}{W_0} \frac{1}{S} = 10 \text{ Log } W/W_0 - 10 \text{ Log } S$$

or

$$(2) \quad IL = PWL - 10 \text{ Log } S$$

The sound pressure level (SPL) actually observed at an arbitrary point in a room is given by the sum of both the reverberant and direct radiated components. Different types of acoustic sources radiate differently depending on the source type and its extent in space. The point source radiates its power symmetrically about any sphere with that source at its center. Because of spherical spreading, the SPL observed drops off 6 dB per doubling of distance from the source. However, for finite line or surface sources this decay with distance is not the same. The works of E. J. Rathe (Reference 3) and R. B. Tatge (Reference 4) deal explicitly with this subject. Close to a line source, SPL drops off at a slow rate, -3dB/doubling. As the distance to the observer becomes much greater than the source length the roll-off increases to the rate of a point source, -6dB/doubling. Tatge developed several curves which plot the roll-off in observed sound pressure level with distance for one circular and several rectangular sources of different aspect ratios. They are non-dimensionalized with respect to distance in terms of the source dimensions and assume that the observer is either over the center of the source or in its plane.

Recalling equation (2), it would be convenient to determine the observed SPL just by adding a correction factor. This factor would account for source shape and the distance and orientation of the observer to it. Rewriting (2):

$$(3) \quad SPL = PWL - 10 \log S + \text{Correction}$$

On the radiating surface, the term would account for pressure doubling. Far away from the source it would show a 6 dB reduction with each doubling

of distance. This is exactly what Tatge does in his work. The curves are derived for radiation normal to a surface's center or in-plane from the mid-point of one edge (See Figure 3). Tatge's curves are in terms of dB. These curves were replotted in terms of their antilogs:

$$C = 10^{\text{Corr.}/10}$$

Equation (3) is then redefined as

$$(3A)\quad SPL = PWL - 10 \text{ Log } S + 10 \text{ Log } C$$

Figures 3-7 plot C for rectangles of 1:1, 2:1, 4:1 and 8:1 aspect ratios and for a circular disk, respectively. Distance is non-dimensionalized in terms of the source's long dimension. One may interpolate between curves to find values of C for intermediate aspect ratios. When the observer point is not directly over the center of the radiating surface, the distance from the point to the source center may be used as an approximation. Equation 3A formulates the direct field due to elementary radiating surfaces and may be used with Figures 3-7 for a given source type and observer location.

When describing how sound is attenuated in passing through a barrier, we speak of the barrier's transmission loss (TL). Transmission loss refers to that portion of the incident pressure that is dissipated or reflected. The wall's sound transmission loss (STL) can be expressed in terms of a transmission coefficient τ:

$$(4)\quad STL = 10 \text{ Log } \frac{1}{\tau}$$

The transmission coefficient τ is really the fraction of the incident pressure that is transmitted through the barrier:

$$(5)\quad \tau = 10^{-(STL/10)}$$

As τ goes to 1, all of the pressure is transmitted and STL goes to 0.

The effective transmission loss (or the effective transmissibility τ_{eff}) of a barrier made up of more than one section lies somewhere between the TL of each individual section. For a barrier of total area S, composed of N sections whose τ's are given by τ_1, $\tau_2 \ldots \tau_N$, the net ETL is given by

$$ETL = 10 \text{ Log } \frac{S}{S_1\tau_1 + S_2\tau_2 + \ldots S_N\tau_N} = 10 \text{ Log } 1/\tau_{eff}$$

This relation can be used to model the presence of an acoustic leak in the panel. Consider a hole (where $\tau = 1$) of some fraction ε of a panel's total area. Assume a uniform transmission loss over the rest of the area (τ_1). Then the effective transmission loss of the entire panel is given by

$$\tau_{eff} = (1-\varepsilon)\tau_1 + \varepsilon$$

Take $\varepsilon = .01$ (1% leakage) as an example. The quantity $1-\varepsilon$ is $.99 \simeq 1.0$; then

$$\tau_{eff} = \tau_1 + .01$$

Note that for a high transmission loss panel, τ is very small. The limiting value of τ_{eff} is .01, meaning that the maximum ETL possible is 20 dB. Should the area of the acoustic leak be anything larger than .1% of the total area, the net ETL of the panel will be dramatically reduced. Figure 8 illustrates the importance of leakage to panel transmission loss performance. It plots the actual TL obtained from a panel designed for a specific value but suffering from leakage effects. From the figure, it is seen that a panel designed for 40 dB attenuation at a specific octave will yield only 20 dB in the presence of 1% leakage. An efficient interior is usually designed for 0.1% leakage.

The sound field inside an aircraft cabin or any other cavity is composed of both direct radiated and reverberant components. Direct radiation, as the name implies, involves only one path between the source and receiver. Reverberation, on the other hand, involves multiple paths because of reflections from the cavity walls. The ability of a wall to absorb sound is the same quality that distinguishes an acoustically "live" (reverberant) room from an acoustically "dead" one. The absorption coefficient α represents that fraction of the incident pressure that is dissipated when the wall would otherwise be a perfect reflector. When very little energy is dissipated at each reflection, the sound pressure in the cavity due to a source can build up to many times the corresponding free-field value. In a highly reflective room, these levels can grow by 10 dB or more. In this case, it is highly advantageous to add absorption. To reduce the internal levels by 10 dB through blockage (transmission loss) might require adding several hundred pounds of interior weight. The addition of absorptive material into the cabin will reduce the reverberant sound field by dissipation at each reflection. To achieve the same reduction using absorption, only a small weight penalty is required since acoustically absorbant materials such as fiberglass batting and polyurethane foams are extremely light.

The acoustic liveness of a room depends upon the room constant R. It is in units of length^2 and represents the area of perfectly absorbent material present in the room. Embelton (Reference 5 - Chapter 9) derives R as follows: The absorption coefficient of a wall at one octave is given by α. If the total surface area of a cavity is given by

$$(6) \quad S_T = \sum_{i=1}^{N} S_i$$

ıen the cavity's average absorption coefficient is defined as

$$(7)\quad \bar{\alpha} = \frac{\sum_{i=1}^{N} S_i(\tau_i + \alpha_i)}{S_T}$$

ıd, subsequently, the room constant becomes

$$(8)\quad R = \frac{S_T\,\bar{\alpha}}{1 - \bar{\alpha}}$$

The Equations of Multibarrier Acoustics

We now have all the tools required to derive the equations governing he propagation of sound through an arbitrary number of cavities. Figure shows a source cavity (0) and an observer cavity (1). The formula that xpresses the impinging sound pressure level SPL_0 on the outlet wall in erms of the source power level PWL_s, source area S_s, room constant R_0, nd directivity/ distance term C_0 is given by

$$(9)\quad SPL_0 = PWL_s - 10 \text{ Log } S_s + 10 \text{ Log } (C_0 + 4/R_0)$$

quation (9) repeats quantitatively that the SPL observed at an arbitrary oint in a cavity is the sum of both the directly radiated and reverberant omponents.

The sound pressure level transferred through barrier 0 into cavity 1 SPL_{01} is given by the impinging sound pressure level SPL_0 minus the arrier's sound transmission loss STL_0, or

$$(10)\quad SPL_{01} = SPL_0 - STL_0$$

$$= PWL_s - 10 \text{ Log } S_s + 10 \text{ Log } (C_0 + 4/R_0) - STL_0$$

Recall STL_0 is given by 10 Log $1/\tau_0$ in equation (4). The power level entering cavity 1 (PWL_{01}) is the intensity times the barrier area, or

$$(11)\quad PWL_{01} = SPL_{01} + 10 \text{ Log } S_0$$

$$(11A)\quad PWL_{01} = PWL_s - 10 \text{ Log } S_s + 10 \text{ Log } (C_0 + 4/R_0) - 10 \text{ Log } 1/\tau_0 + 10 \text{ Log } S_0$$

PWL_{01} is now the sound power source in cavity 1. Again applying Equation (9), the SPL impinging on the observer in cavity 1 (SPL_1) is given by

$$(12)\quad SPL_1 = PWL_{01} - 10 \text{ Log } S_0 + 10 \text{ Log } (C_1 + 4/R_1)$$

By substituting equation (11A) SPL_1 may be expressed in terms of the original source power level

$$(13)\quad SPL_1 = PWL_s - 10 \text{ Log } S_s + 10 \text{ Log } (C_0 + 4/R_0) + 10 \text{ Log } \tau_0 + 10 \text{ Log } (C_1 + 4/R_1)$$

As more cavities are added, the terms can be grouped together. For N cavities, the sound pressure level in cavity N is given by

$$(14)\quad SPL_N = PWL_s - 10 \text{ Log } S_s + 10 \text{ Log } \left[(C_0 + 4/R_0)(C_1 + 4/R_1) \ldots (C_N + 4/R_N)\right] + 10 \text{ Log } \left[(\tau_0)(\tau_1)(\tau_2) \ldots (\tau_{N-1})\right]$$

It is interesting to consider some limiting cases. As STL→0, τ→1. If there were no barriers, the product of all the τ's would be 1. Since Log(1) = 0, there would be zero barrier attenuation. As the walls become either more transparent or absorptive, R grows larger and the component due to reverberant build-up disappears. Comparing the relative magnitude of the terms C and 4/R will show whether direct radiation or reverberation dominates the sound field. The proper treatment for noise reduction becomes apparent. Adding absorption will reduce the reverberant component only, while adding transmission loss will reduce the direct radiation. This points out the need for a balanced treatment, in that over-treating one component does nothing for the other. Should the source impinging on S_0 be in the open air, such as with rotor noise, SPL_0 reduces to

$$(15)\quad SPL_0 = PWL_s - 10 \text{ Log } S_s + 10 \text{ Log } C_0$$

Hence, when there is no source cavity and the sound pressure level impinging on wall S_0 is already known, the terms in equation (14) that are on the right hand side of equation (15) can be replaced simply with SPL_0.

Structural Radiation

Radiation by structural members is difficult to predict without measured values of structural impedance or mobility. Point (attachments), line (frames, stringers), and surface (skin) sources contribute to the total picture of structural radiation. Rather than attempt to identify each component, a more statistical approach should be used. Whole surfaces are assumed to radiate instead of discrete parts. The power fed

ıto the cabin by the source is distributed among the individual radiating ırfaces. The resulting intensity distribution on each surface (power/unit ːea) is assumed to be uniform.

When more than one surface within a cavity radiates, the expression ɔr the SPL at the observer can become very complex. Some simplification ɑn be accomplished by expressing the radiation intensity of the surfaces ı terms of that of one surface. The total intensity observed at one ɔsition is the sum of the intensities propagated from each surface. If ıere are N surfaces of area S_1, S_2, ... S_N radiating power W_1, W_2, ... N then the total intensity observed is

$$(16)\quad I_{obs} = \frac{W_1}{S_1} \cdot C_1 + \frac{W_2}{S_2} \cdot C_2 + \ldots + \frac{W_N}{S_N} \cdot C_N$$

here C_1, C_2, ... C_N represent the directivity factors for the radiating urfaces. Define a radiation intensity ratio $\rho_i = \frac{W_1/S_1}{W_i/S_i}$. Equation (16) ɑn be rewritten

$$(17)\quad I_{obs} = \frac{W_1}{S_1} \left[C_1 + C_2/\rho_2 + \ldots + C_N/\rho_N \right]$$

hen the level is given by

$$(18)\quad SPL_{obs} = PWL_1 - 10 \text{ Log } S_1 + 10 \text{ Log } \left[C_1 + C_2/\rho_2 + \ldots + C_N/\rho_N \right]$$

The ratio ρ_i is really the ratio of the intensity of wall 1 to the .ntensity of wall i. If we assume that the intensity level drops 6 dB at ı corner or intersection with a heavy frame, as illustrated in Reference ɔ, Chapter 11, we are saying that the intensity is cut in half. In other ɾords, the radiation ratio $1/\rho_i$ equals 1/2. This greatly simplifies the ːquation for the total intensity observed. A generalized expression for ɜtructural radiation that includes panel transmission loss and room ɑcoustics follows:

$$(19)\quad SPL_{obs} = PWL_1 - 10 \text{ Log } S_1 + 10 \text{ Log } \left[\tau_1 (C_1 + 4/R) + \frac{\tau_2 (C_2 + 4/R)}{\rho_2} + \ldots + \frac{\tau_N (C_N + 4/R)}{\rho_N} \right]$$

SOURCE STRENGTH PREDICTION OF MAJOR COMPONENTS

A guide to the prediction of noise generated by the major helicopter noise sources is presented. Trends are shown over a wide range of operating parameters. Specific examples are given based on the prediction of noise in the NASA/Sikorsky Civil Helicopter Research Aircraft (CHRA), a modified CH-53 A/D. The CHRA is a six bladed, single main rotor helicopter in the 15 900 kg (35,000 lb) weight class, powered by two G.E. T-64 engines.

Transmission Noise

The prediction of gear noise remains the most challenging of all the aspects of helicopter internal noise. Recent work by Grande et al (Reference 6) has demonstrated consistent trends with such variables as horsepower, specific tooth load, pitch-line velocity, manufacturing tolerances, and gear type. Other studies (Reference 7) attempt to correlate with the noise field surrounding the gearbox casing. NASTRAN® and other finite element models are just now being used at acoustic frequencies to analytically predict frequency response and acoustic radiation (Reference 8). It would be a difficult enough problem if the noise radiation stopped at the gearbox casing feet: a problem in direct radiation. However, the casing is mounted to an arbitrary airframe which is driven by the casing's foot motions: a problem in structure-borne noise. Differing airframe geometries, casing designs, and gearbox mounting techniques add a new set of variables to the noise problem. Figure 10 shows the trend in bare cabin gear clash tones with a variety of gearbox mounting types. The curves show the influence of the propagation path from the primary gear clash source to the radiating airframe. Scatter in the data can be attributed to local (but significant) frame resonances.

How, then, can the designer determine the cabin noise levels generated by the main transmission in an arbitrary helicopter? Some assumptions must be made about the propagation of structure-borne noise along the airframe. When driven by a gearbox foot, a heavy structure such as a forging will tend to radiate along its entire length. Intersections between heavy structure and light structure (skins and stringers) tend to reject structure-borne noise because of the impedance mis-match.

Beraneck considers the problem of the attenuation of structure-borne noise at corners and intersections (Reference 5, Chapter 11). He assumes that, with the same structural properties on either side of a 90° turn, a 3 dB attenuation in power will be observed. Similarly, crossing over a heavy frame is assumed to give a 3 dB reduction. On this basis, the analyst can examine the aircraft structure and establish the radiating areas.

As an example, figure 11 illustrates the radiating areas used to model the CHRA structure-borne noise induced by the main transmission. The model resulted from a review of the CHRA NASTRAN work performed by M. W. Dean (Reference 9). The primary area of radiation is the ceiling from

tation 282 to station 442. The frame at STA 442 is a major forging and erves to carry the landing gear loads. The frame at STA 282 is also a ajor structure and carries the engine support loads. Beyond these tations, a 3 dB reduction in intensity is assumed. These areas are ounded forward by the cockpit bulkhead (STA 162) and aft by the tailcone ntersection (STA 522). Radiation from the sidewalls is assumed to xtend from the ceiling (waterline 191) down to the sponson intersection t waterline 132. The presence of the full cell and additional supporting tructure within the sponson is assumed to stiffen the lower sidewall ufficiently to eliminate its radiation of structure-borne noise.

In the absence of a detailed prediction scheme, some trends can be eveloped based on measurements taken in untreated CH-53 aircraft. igure 12 plots the observed relation between the total radiated acoustic ower within the cabin at each gear clash fundamental and the consumed P. This plot was derived from typical CH-53 data measured at Sikorsky. here are separate lines for the three major gear types in the main ransmission. For the CH-53D, the phased 2nd stage planetary gears enerate nearly 15 dB less acoustic power than the unphased first stage lanetaries. The main bevel is another 5 dB down from the second stage lanetary level.

As discussed in the section on structural radiation, the observed ound pressure levels can be determined from the radiation intensity of he dominant surface ($PWL_1 - 10 \text{ Log } S_1$), the room constant R_1, and irectivity/distance factors C_i (equation 22). The value of the sound ower level radiated by the dominant overhead region can be expressed in erms of the total power (From Figure 11) and the area ratios of the econdary regions. If the total power radiated by the structure is given y

$$(20)\quad W_T = W_1 + W_2 + \ldots + W_N$$

nd if the intensity ratio between the dominant (1) and secondary surfaces i) is assumed to be

$$(W_i/S_i)/(W_1/S_1) = 1/2$$

r

$$\frac{W_i}{W_1} = \frac{S_i}{S_1}\frac{1}{2} = \frac{\sigma_i}{2}$$

hen the total power radiated into the cabin by N surfaces can be expressed as

$$(21)\quad W_T = W_1\ (1 + \sigma_2/2 + \ldots + \sigma_N/2)$$

and

$$(22)\quad PWL_T = PWL_1 + 10 \text{ Log } (1 + \frac{\sigma_2}{2} + \ldots + \frac{\sigma_N}{2})$$

Finally, the sound power level radiated by the dominant area (PWL_1) in terms of the total power from Figure 12 (PWL_T) is

$$(23)\ PWL_1 = PWL_T - 10\ Log\ (1 + \frac{\sigma_2}{2} + \ldots + \frac{\sigma_N}{2})$$

This equation expresses the acoustic power radiated by the dominant ceiling area in terms of the total acoustic power associated with the gearbox. The gear noise octave spectrum can be generated by calculating the harmonic frequencies of each gear and applying the generalized harmonic spectrum of Figure 13. This spectrum was developed from the findings of Grande, et al. in Reference 6 and agrees well with observed CH-53D data. Once the harmonic frequencies and levels are determined, the total octave levels can be summed according to the bands into which the harmonics fall.

For example, the CH-53D consumes 3.7 MW (5000 HP) (approximately) in both 150 knot cruise and hover at sea level, operating near 15 900 kg (35 000 lb) gross weight. Figure 12 indicates that the acoustic power radiated at the fundamental gear clash frequencies are 134, 118.5, and 115 dB for the first stage planetaries, second stage planetaries, and main bevel gear, respectively. Gear noise harmonics occur at multiples of the first stage gear clash frequency of 527 Hz, and bevel clash frequency of 2710 Hz.

The following table of power levels summarizes the construction of the octave spectrum:

TOTAL ACOUSTIC POWER - PWL_T

Octave Level - dB

Gear	500 Hz	1000 Hz	2000 Hz	4000 Hz	8000 Hz
2nd Pl.	118.5	118.5	103.5	103.5	93.5
1st Pl.	--	134.5	134.5	119.5 119.5	109.5 109.5
Bevel	--	--	115.5	115.5	100.5 100.5
Sum	118.5	134.5	134.5	123.3	113.0

The above table refers to the total structure-borne acoustic power radiated in each octave because of the main transmission. Only a small percentage of this total power is radiated by the transmission casing

tself due to its relatively small exposed area and the fact that it is overed by a rubber drip pan. Most of it is radiated by the cabin ceiling, idewalls, and frame members. Substitute PWL_T into equation (23) to etermine PWL_1. Substitute PWL_1 into equation (19) to determine cabin oise levels.

Engine Noise

A review of turboshaft engine noise radiated by inlet, casing, and xhaust reveals consistent trends with horsepower. Figure 14 shows the ound power level radiated by several types of turboshaft engines over a ide range of horsepower. This chart, derived from Reference 6 and dditional Sikorsky data, follows the relation PWL = 10 Log(HP) + 108 dB. ost of the noise is radiated by the casing and exhaust except when the ngine blade passage frequency falls within the 8000 Hz octave. Then nlet noise will dominate the uppermost octave. With the current CH-3A/D engine installation, inlet noise is not heard in the passenger abin. Therefore, inlet noise was not considered a major source in the HRA cabin. By overlaying the spectra of the engines onto one plot ormalized by HP, a close correspondence in shape was noted. A conserva-ive, generalized spectral shape was averaged through the upper limit of he data for casing, exhaust, and inlet power levels. These are plotted n Figures 15, 16, and 17. By adding 10 Log (HP) to these non-dimension-.lized spectra, a close estimate of the engine octave power levels can be btained. Note that the T-64 is quieter in the lower octaves than the eneralized spectrum. To calculate the engine noise radiated into the .ircraft cabin, the radiating areas must be determined. The firewall ransmits the casing noise while the aircraft skin aft of the engine acelle transmits the exhaust noise. The calculation procedure for ngine casing noise is demonstrated in the sample problem later in the aper. Exhaust noise contours are plotted in Figure 18. Note that the .evels fall off sharply in the near-field: 15 dB down at a distance of wo exhaust diameters.

Rotor Noise

Few methods exist for the prediction of near-field rotor noise. utherland and Brown (Reference 10) provide an excellent technique for letermining blade passage harmonic levels within a radius of one rotor iameter. It has been applied successfully to the prediction of both ain and tail rotor noise. The method is adequately explained in Reference 10 and will not be reproduced here. What is required is a means of predicting near-field rotor broadband noise in terms of octave bands. Many computer programs exist for the prediction of rotor noise in the far-field. The method employed at Sikorsky Aircraft is based on the Lowson and Ollerhead rotor rotational noise program (Reference 11) modified by C. L. Munch to also predict rotor broadband noise (Reference 12). The method has since been updated to include the effects of blade twist based on extensive whirlstand testing. A graphical representation of this method was prepared by W. Bausch of Sikorsky Aircraft and was included in a comprehensive V/STOL noise prediction report authored by B. Magliozzi

(Reference 13). The approach taken will be to use this method to calculate both rotor rotational and broadband noise in the far-field and correct it back to near-field levels. The observer position will be on-axis to further simplify the equations.

Broadband Noise

Rotor broadband noise is a function of tip speed (V_t), thrust (T), total blade area (A_b), blade linear equivalent twist (θ), and distance to the observer (R). On the rotor axis, this relation is given by

$$SPL_{bb} = 20 \text{ Log } V_t + 20 \text{ Log } T - 10 \text{ Log } A_b - .56\ (\theta) - 20 \text{ Log } R + 21.9$$

This represents the overall rotor broadband noise level. To obtain the octave levels, a generalized spectrum shape based on the rotor Strouhal frequency is used. Rotor broadband noise has long been associated with the unsteady vortex shedding at the airfoil trailing edge. The exact mechanism is not clear but a scaling with Reynolds number is observed, hence the association with vortex shedding. The frequency of peak broadband noise (f_s) is well predicted in terms of blade chord (c), thickness (t) and velocity

$$f_s = .28 \frac{V_{.7}}{h_1}$$

where $h_1 = c \sin \theta_{.7} + t \cos \theta_{.7}$

and $V_{.7}$ and $\theta_{.7}$ represent the velocity and blade angle of attack at the 70% radius, respectively.

It is convenient to set the peak frequency to the closest octave center frequency. For example, if f_s is found to be 225 Hz, set it equal to 250 Hz. Using the generalized octave spectrum of Figure 19, the individual octave levels, SPL_{OCT}, are determined by adding the corresponding band level SPL_{BL} to the overall broadband level, SPL_{OA}

$$SPL_{OCT} = SPL_{OA} + SPL_{BL}$$

Rotational Noise

The harmonics of blade passage for a hovering rotor can be determined from thrust, torque, tip speed, and twist. Because the thrust term dominates on-axis, the torque component will be neglected. Obtain the partial level SPL_T from Figure 20 corresponding to the rotor thrust (T). For each harmonic, m, calculate mB and find the corresponding partial level SPL_m from Figure 21. Find the correction for blade twist, SPL_θ from Figure 22. The sum of these partial levels for one harmonic, SPL_{mB},

epresents the total on-axis level for a hovering rotor at a distance of 00 ft. At any distance, R

$$SPL_{mB} = SPL_T + SPL_m + SPL_\Theta + 20 \text{ Log } (\frac{R}{200})$$

The total rotor noise octave spectrum is obtained by adding the otor harmonics in each octave, logarithmically, and combining these with he respective broadband levels. In general, rotor noise dominates only he lowest octaves. This is because of the rapid roll-off of rotor armonics and the small amount of transmission loss provided by structural aterials at low frequencies.

The problem now is to translate far-field octave band data into the ear-field. This can be accomplished by using the distance/directivity urve for a circular source from Figure 7. By taking the noise measured or predicted) on the rotor centerline at 10 rotor diameters, and then oving the levels in on the curve to the desired distance below the rotor ead, an approximation to the near-field rotor spectrum is obtained. One important assumption is made for rotor noise very close to the rotor disk. Because a rotor is not a solid surface radiator, it is assumed that C can e no larger than 1.0. Realistically, there is no pressure doubling in space as there is near a wall. In equation form,

$$(24)\ SPL_{near} = SPL_{far} + 10 \text{ Log } \frac{C(r_1/L)}{C(r_2/L)}$$

where r_2 is the far-field distance, r_1 is the near-field distance, and L is the rotor diameter. As an example, let L = 72 ft. If the octave level measured at 720 ft is 100 dB and the level 7.2 ft under the rotor is desired, then

$$SPL_{near} = 100 + 10 \text{ Log } \frac{C(7.2/72)}{C(720/72)}$$

Going to curve 1 of Figure 7, C(.1) = 1.8 and C(10) = .001. However, C cannot be greater than 1.0, so take C(.1) = 1.0. Then 10 Log (1.0/.001) = 30 and

$$SPL_{near} = 100 + 30 = 130$$

Note that using a simple 6 dB/doubling of distance relation would have given 140 dB for the near-field level. This technique can also be used for tail rotors when in-plane levels are required by obtaining C from curve 2 of Figure 7.

Boundary Layer Noise

In high speed flight, boundary layer noise can be a significant part of the noise observed in the aircraft cabin. Airframe noise is generated by any part of the aircraft structure protruding into the flow. It can

be especially intense when generated by struts, flaps, doors, or open cavities. However, the detailed prediction of airframe noise is beyond the scope of this report and will not be dealt with. The CH-53D aircraft is relatively clean in the airframe sense, with no major sources. Only the noise generated by the turbulent boundary layer will be considered. The method used for calculating boundary layer noise is due to Bies (Reference 14). His work is a summary of wind tunnel and aircraft measurements made of turbulent boundary layer pressure fluctuations over a wide range of Reynolds and Mach numbers.

The procedure is summarized as follows. Calculate the overall fluctuating pressure levels from the equation

$$(25) \qquad FPL_{overall} = 20 \text{ Log } q + 84 \quad dB$$

where q is the free stream dynamic pressure $1/2\rho U_\infty^2$. The boundary layer displacement thickness is approximated by

$$(26) \qquad \delta^* = 0.0016 \text{ X}$$

where X is the distance from the leading edge (assumed greater than 10 ft). The characteristic frequency is determined from

$$(27) \qquad f_o = 0.1 \text{ } U_\infty/\delta^*$$

Figure 23 plots the non-dimensionalized fluctuating pressure levels Δ in 1 Hz octave bands. To determine the dimensional octave levels, use the following equations:

$$(28) \qquad SPL_{1Hz} = FPL_{overall} - 10 \text{ Log } f_o + \Delta$$

$$(29) \qquad SPL_{octave} = SPL_{1Hz} + 10 \text{ Log } (bw)_{octave}$$

where the octave bandwidth (bw) is given by $\frac{\sqrt{2}}{2}$ times the octave center frequency.

The following example calculated the boundary layer noise at station 342 on the CHRA fuselage at 150 knots (253.5 ft/sec). The dynamic pressure q is

$$q = 1/2 \text{ } (.00238) \text{ } (253.5)^2 = 76.5 \text{ lb/ft}^2$$

$$FPL_{overall} = 20 \text{ Log } (76.5) + 84 = 121.7 \text{ dB}$$

The boundary layer momentum thickness is

$$\delta = 0.0016 \text{ } (21) = 0.0336 \text{ ft}$$

$_o$ is then given by

$$f_o = 0.1\ (253.5/0.0336) = 754.5\ \text{Hz}$$

he following table lists the values of Δ obtained from Figure 23, the alues of SPL_{1Hz}, and the octave levels:

Octave frequency	$\%f_o$	Δ	SPL_{1Hz}	10 Log(bw)	SPL_{octave}
31.5	.04	-3	90	15	105
63	.08	-3	90	18	108
125	.17	-3	90	21	111
250	.33	-4	89	24	113
500	.67	-5	88	27	115
1000	1.34	-7	86	30	116
2000	1.67	-10	80	33	113
4000	5.30	-14	76	36	112
8000	10.60	-20	70	39	109

The SPL's of the above table indicate the fluctuating pressure levels on the outside skin induced by the turbulent boundary layer.

INTEGRATED METHOD

Checklist

A step-by-step checklist is presented below to summarize the process of translating an external source strength into an internal noise level.

1. Define aircraft structure and geometry.
2. Identify the major sources and paths.
3. Define the source strengths at the required operating parameters.
   a. Engine noise from Figures 14-18 and Equation (14).
   b. Gearbox noise from Figure 12 and Equations (23) and (19).
   c. Rotor noise from near-field data and Figure 7.
   d. Boundary layer noise from Equations (25)-(29).

4. Translate the source strengths into the cabin using Equation (14) or (19) as required:

   a. Determine C_i's from radiating surface size and distance to the observer via Figures 3-7.

   b. Obtain transmission loss data from a data base.

   c. Calculate room constant data from cabin dimensions and Equations (6) - (8).

   d. Apply Equation (14) or (19) octave by octave.

5. Tabulate and sum the octave data from each source and path to obtain total observed sound pressure level.

Application to Engine Casing Noise

The use of the equations of multibarrier acoustics will be demonstrated by working through the calculation of engine casing noise in the bare aircraft cabin (Figure 24). Figure 25 presents an idealization of the engine/nacelle arrangement. Having engineering drawings of the installation is essential in determining the physical dimensions required for the calculations. The complicated arrangement can be simplified by making a few assumptions. First, let the nacelle be a rectangular structure with the firewall corresponding to the outlet wall b_0. Next, let the source be a flat surface with dimensions equal to the engine's average cross-section. Faces a_0, e_0, and f_0 can be combined since they represent the cylindrical nacelle fairing. Face d_0 reduces to an open annulus around the tail pipe extension that serves as the engine cooling air exit. Face c_0 includes the surface area of the engine (which acts as an inner wall) as well as the fiberglass engine intake duct.

The nacelle fairing is made of reinforced fiberglass approximately 0.838 mm (0.033 in.) thick. There is one fire-fighting access hole in the fairing. The firewall, integral with the aircraft skin, is made of titanium The presence of numerous stiffeners and doublers makes it necessary to use two average values of firewall thickness. Engineering prints indicate that 0.457 and 1.09 mm (0.018 and 0.043 in.) are appropriate values. The proportions are 59% and 41%, respectively. Geometric parameters come from the engineering drawings. Some allowances must also be made for leakage through access holes and joints. One percent has been found to be a good approximation.

Consider the nacelle cavity at the 31.5 Hz octave. Table I summarizes the data and shows how the room constant is calculated for that octave. Most of the walls are made up of two different materials. Wall a_0 (nacelle fairing) is built of .033 fiberglass (69.8 ft^2 area) but also has a fire-fighting access hole (.34 ft^2) in it. This serves to reduce the net trans-

ission loss of the wall. To calculate the effective transmission loss (ETL) f a composite panel, use the relation

$$\frac{1}{\tau} = \frac{S_T}{S_1\tau_1 + S_2\tau_2}$$

ad

$$ETL = 10 \text{ Log } \frac{1}{\tau}$$

The absorption coefficient α for fiberglass at 31.5 Hz is .02. Then $+ \alpha$ is 0.72. Multiplying by the fairing area (70.1 ft^2) then $S(\tau + \alpha)$ s 50.4 ft^2. Repeating the process for the other walls, the room constant R t 31.5 Hz is calculated to be 101 ft^2.

Following the path of transmission into cavity 1, the directivity/ istance function C_0 must be determined to find the level impinging on utlet wall b_0. The engine is approximately a 3 x 1 rectangle with long ide dimension 6.7 ft. The distance r/L is 1.9/6.7 = 0.28. There is o chart for C for a 3/1 rectangle, so the average of the 2/1 and 4/1 alues must be taken. C_{avg} is 0.37. Table I shows that the ETL of the irewall (b_0) is 9.7 dB and τ = .108 at 31.5 Hz. All that remains is to ind the distance/directivity factor C_1 to account for the propogation f the casing noise from the firewall to the cabin center. Figure 25 shows hat the firewall is a 6 x 1 rectangle with long dimension 8.3 ft. etting the observer be positioned under the main transmission, r/L ecomes 4.4/8.3 = 0.53. Taking the average between the 4/1 and 8/1 ectangular source curves, C_1 is 0.085. The work sheet of table II ummarizes all of the data for each octave including the casing power evel from the source strength data base. Source 0 on the work sheet is he engine itself, while Source 1 is the firewall. All of the required nformation is known and can now be entered into Equation (14). The esulting SPL's are listed in the last column.

CORRELATION

The method was applied to the prediction of CHRA internal noise for oth the treated and untreated cases. The model included main rotor, tail rotor, engine, main transmission and boundary layer noise.

The noise levels predicted in the bare cabin agree very well with the measured data as shown in Figures 26-27. The best correlation exists in the middle octaves which are dominated by gear noise. The SIL is predicted within 1.2 dB. The lower octaves are high by 2-4 dB in hover. This is due to an overprediction of main rotor noise which controls the level of these octaves. This points out the shortcomings of using a uniform, circular source to approximate a rotor disc. The correlation improves in cruise. The upper octaves are underpredicted by as much as 10 dB in both hover and cruise. A review of the narrow-band spectra at these

flight conditions confirmed the existence of these high broadband levels over the gear clash harmonic tones. It is significant that this occurs at such high frequencies. Because of the large amount of transmission loss associated with most materials at the upper octaves, these upper octave levels should be very low. This implies that there is some direct radiatio from the skin surface or through a leak. The one source that could provide the necessary levels at the upper octaves is the engine. It is likely that engine-induced vibration was being fed to the firewall and surrounding frames via the engine mounts and forced structural radiation in this area. Engine-induced structure-borne noise was not considered in the calculations because of a lack of the appropriate data.

Correlation of the treated cabin levels shows some interesting effects (Figures 28 and 29). Predicted and measured levels agree very well in the upper octaves, unlike the bare aircraft case. This tends to confirm the contention that engine-induced vibration is being radiated by the skins or frames. The 500 Hz octave is underpredicted by 6 dB. This is due to the fact that the aft bulkhead was radiating a significant amount of structure-borne noise. This was confirmed during flight tests of the treated CHRA when a lead-vinyl curtain was placed over the bulkhead. The levels observed in the gear noise-dominated octaves dropped 2-6 dB. The levels in the 125-500 Hz octaves are underpredicted. This frequency region is dominated by main rotor and engine casing noise implying that there was some sort of leakage or panel resonance. It is probable that these sources entered the ECU ducting behind the valances. The treatment is not continuous over the frames where the valances are attached. Since there is not treatment within the ECU ducts, any noise entering would be free to propagate along the length of the ducting. The contribution of the ECU system was not included in the noise prediction method because an adequate model was not yet available.

Overall, the correlation of predicted levels with measured data is excellent. Comparisons indicate that the method could be improved by adding the effects of engine-induced structure-borne noise and developing a procedure that would account for the ECU ducting.

CONCLUSIONS

1. The integrated method presented provides an easily workable and correlated procedure for the prediction of helicopter internal noise. The method is sufficiently general to be applicable to helicopters and other aircraft types when the appropriate structural geometry, noise source strengths, and material acoustic properties are defined.

2. The levels predicted by the method for the CHRA correlate well with measured data in both hover and cruise. The hover SIL was predicted within 1.2 dB for the bare aircraft and 0.1 dB for the treated aircraft. In cruise, the SIL correlated within 0.2 dB for the bare aircraft and within 1.2 dB for the treated case.

3. An accurate definition of the problem is essential for good correlation between measured and predicted levels. This includes the definition of structural geometry, a proper identification of the paths of propagation, a correct estimate of source strengths, and an accurate data base of material acoustic properties (transmission loss and absorption).

4. The approximation of a uniform circular source distribution for near-field rotor noise used in this procedure was shown to slightly over-predict the levels very close to the rotor disc. A more exact model is required that accounts for the fact that most of the acoustic energy is generated by the outboard sections of the rotor disc and is not uniformly distributed.

REFERENCES

1. Levine, L. S. and DeFelice, J. J., "Civil Helicopter Research Aircraft Internal Noise Prediction", NASA Contractor Report, NASA CR-145146, April 1977.

2. USA Standards Institute: USAS-S1.6-1967 Preferred Frequencies and Band Numbers for Acoustical Measurement, 1967

3. Rathe, E. J., "Note on Two Common Problems of Sound Propagation," Journal of Sound and Vibration, 10(3), 472-479, 1969

4. Tatge, R. B., "Noise Radiation by Plane Arrays of Incoherant Sources, JASA Volume 52, Number 3 (Part I), 1972

5. Beranek, L. L., "Noise and Vibration Control", McGraw-Hill Book Company, 1971.

6. Grande, E. and Brown, D., "Small Engine Noise Prediction," Technical Report AFAPL-TR-73-79, Volume II, December 1973

7. Bowes, M. A., Giansante, N; "Helicopter Transmission Vibration and Noise Reduction Program", USAAMRDL-TR-77.14, June 1977.

8. Howells, R. W. and Sciarra, J. J., "Finite Element Analysis Using NASTRAN Applied to Transmission Vibration/Noise Reduction", Paper presented at Fourth NASTRAN Users' Colloquium at NASA-Langley Researc Center (NASA-TMX-3278), September 1975.

9. Dean, M. W., "Correlation of an Extended CH-53 Helicopter Nastran Model with Full Scale Aircraft Shake Test Data," NASA Contractor Report, NASA CR-145012, July 1976

10. Sutherland, L. C. and Brown, D., "Prediction Methods for Near Field Noise Environments of VTOL Aircraft," AFFDL-TR-71-180, May 1972

11. Lowson, M. V. and Ollerhead, J. B., "Studies of Helicopter Rotor Noise," USAAVLABS Technical Report 68-60, January 1969

12. Munch, C. L., "Prediction of V/STOL Noise for Application to Communit Noise Exposure," Dept. of Transportation Report DOT-TSC-OST-73-19, May 1973

13. Magliozzi, B., "V/STOL Rotary Propulsion Systems Noise Prediction and Reduction," Dept. of Transportation, FAA Systems Research and Development Service Report FAA-RD-76-49, May 1976

14. Bies, D. A., "A Review of Flight and Wind Tunnel Measurements of Boundary Layer Pressure Fluctuations and Induced Structural Response, NASA Contractor Report, NASA CR-626, October 1966

TABLE I.- CAVITY AND WALL NOMENCLATURE

WALL	A	B	C	D	E	F
$S(ft^2)$	70.1	11	73	.62		
S_1	69.8	4.5	10	.62		
ETL_1	1.5	14.5	1.5	0		
τ_1	.7	.035	.7	1		
S_2	.34	6.5	63			
ETL_2	0	8	27			
$\bar{\tau}_2$	1	.158	.0012			
ETL	1.5	9.7	10.1	0		
τ_{eff}	.7	.108	.097	1		
α	.02	.02	.02	0		
$\tau_{eff}+\alpha$	.72	.128	.117	1		
$S(\tau_{eff}+\alpha)$	50.4	1.41	8.5	.62		

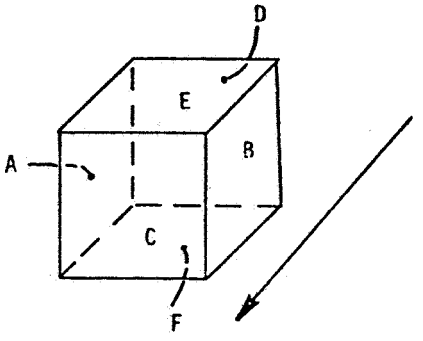

A - OUTBOARD
B - INBOARD
C - FORWARD
D - AFT
E - UPPER
F - LOWER

$S_T = \sum_{i=a}^{f} S_i$	ft^2	154
$S\bar{\alpha} = \sum_{i=a}^{f} S_i(\tau_i + \alpha_i)$	ft^2	61
$\bar{\alpha} = \frac{\sum_{i=a}^{f} S_i(\tau_i + \alpha_i)}{S_T}$		0.396
$R = \frac{S\bar{\alpha}}{1-\bar{\alpha}}$	ft^2	101

NOTE: For tone dominance use transmission loss at tone frequency.

$1\ ft^2 = .093\ m^2$

DIMENSIONS LISTED IN FEET FOR COMPATIBILITY WITH BARRIER EQUATIONS

TABLE II.- ENGINE CASING NOISE - BARE AIRCRAFT

BASIC DATA

OCTAVE	R_0	R_1	R_2	C_0+4/R_0	C_1+4/R_1	C_2+4/R_2	τ_1	τ_2
31.5	101	95		.41	.13		.108	
63	86.5	95		.41	.13		.11	
125	56.9	78		.44	.14		.068	
250	18	54		.59	.15		.022	
500	7.2	50		.93	.17		.011	
1K	5.29	53		1.1	.16		.007	
2K	4.41	54		1.3	.16		.0021	
4K	5.9	68		1.0	.14		.0018	
8K	7.49	70		.9	.14		.0007	

SOURCE	AREA ft^2	TYPE	C
0	10.2	RECT.	.37
1	10.2	RECT.	.085
2			

* REFERENCE EQUATION (14)

$1\ ft^2 = .093\ m^2$

DIMENSIONS LISTED IN FEET FOR COMPATIBILITY WITH BARRIER EQUATIONS

SUMMARY CALCULATION*

OCTAVE	SPL or PWL	PWL $-10 \log S$	$10 \log (C_0+4/R_0)(C_1+4/R_1)(C_2+4/R_2)$	$10 \log \tau_1 \cdot \tau_2$				SPL_{obs}
31.5	118.8	108.7	-12.7	-9.7				86.3
63	126.8	116.7	-12.7	-9.6				94.3
125	129.8	119.7	-12.1	-11.7				95.9
250	130.3	120.2	-10.5	-16.6				93.1
500	130.8	120.7	-8	-19.6				93.1
1K	127.8	117.7	-7.5	-21.5				88.7
2K	128.8	118.7	-6.8	-26.8				85.1
4K	127.8	117.7	-8.5	-27.4				81.8
8K	132.3	122.1	-9	-31.5				81.8

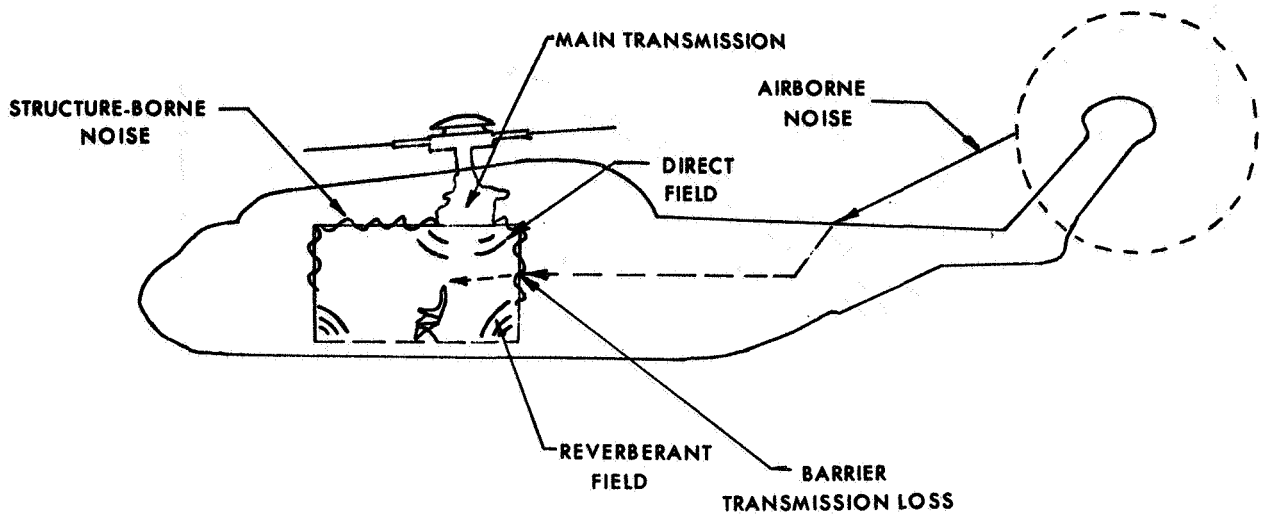

Figure 1.- Modes of propagation for cabin noise.

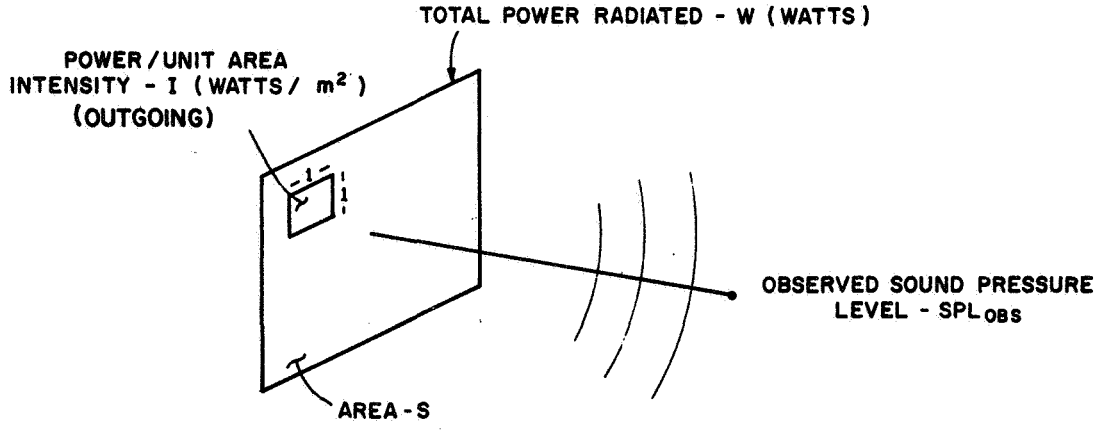

$$IL = 10 \log \frac{I}{I_o}$$

$$PWL = IL + 10 \log S$$

$$SPL = PWL - 10 \log S + 10 \log C$$

Figure 2.- The relation of PWL, IL, and SPL for a plane source.

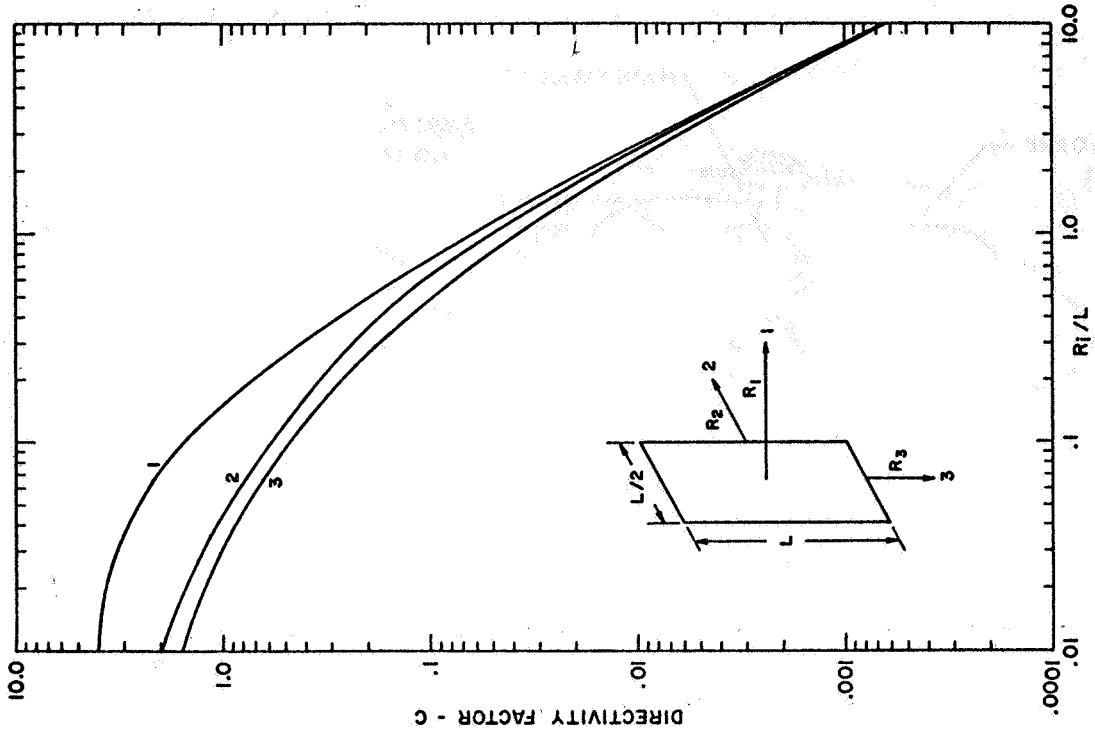

Figure 4.- Directivity factor for a rectangular plate (2/1).

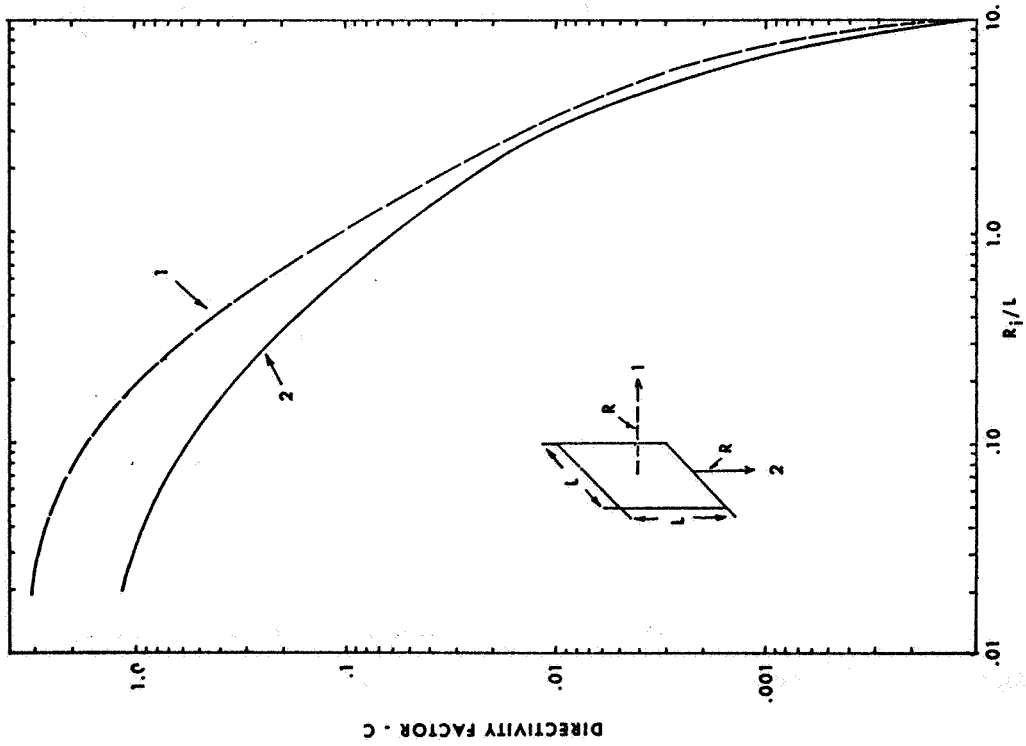

Figure 3.- Directivity factor for a square plate.

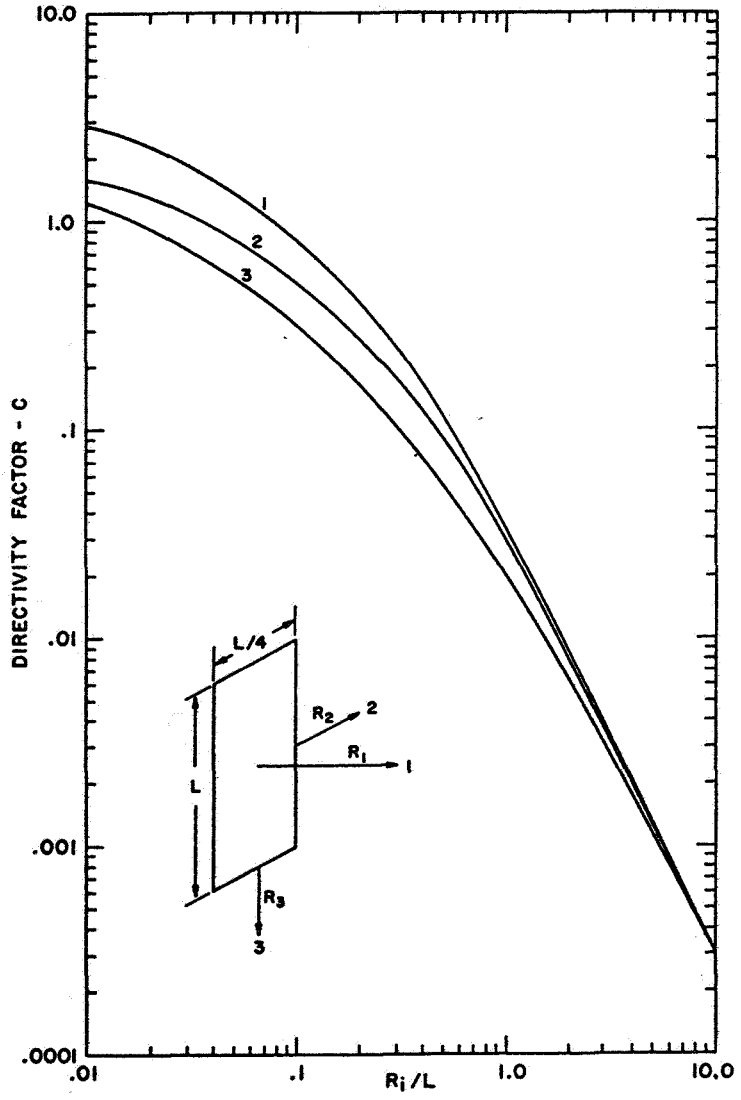

Figure 5.- Directivity factor for a rectangular plate (4/1).

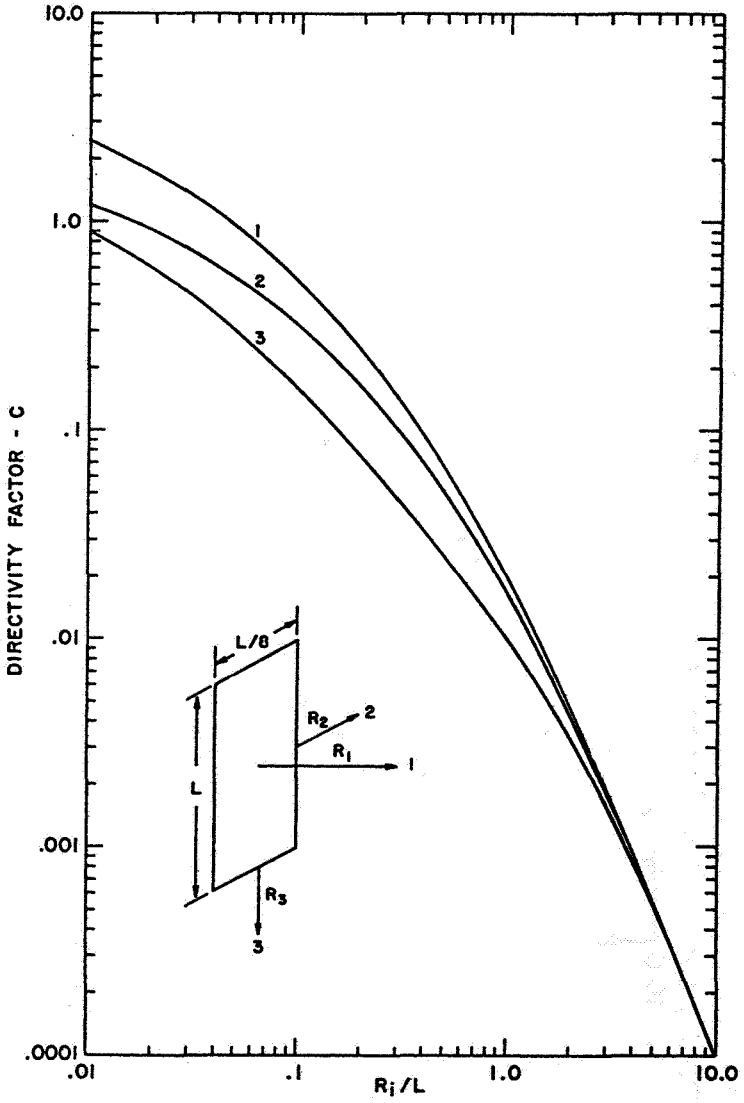

Figure 6.- Directivity factor for a rectangular plate (8/1).

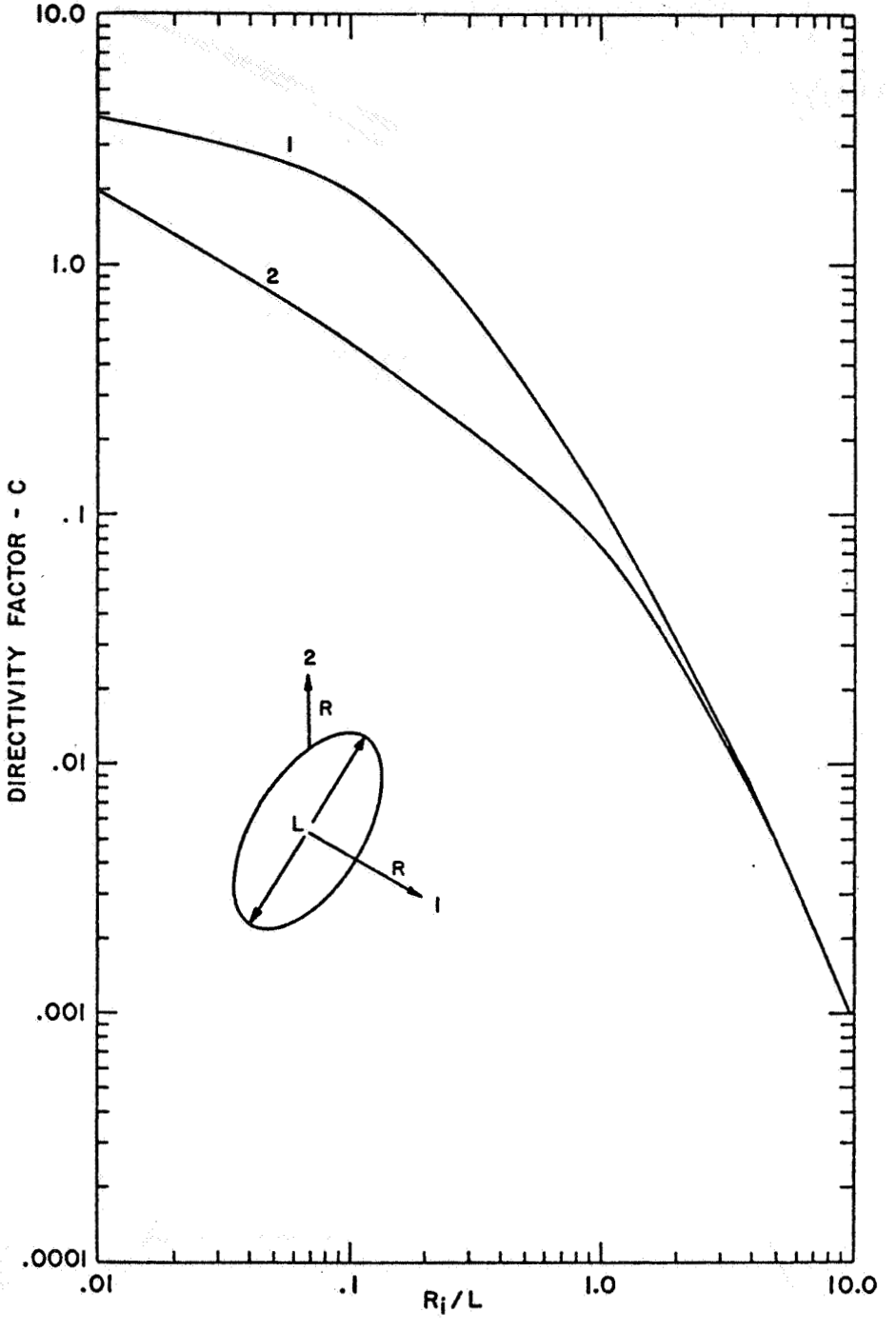

Figure 7.- Directivity factor for a circular disk.

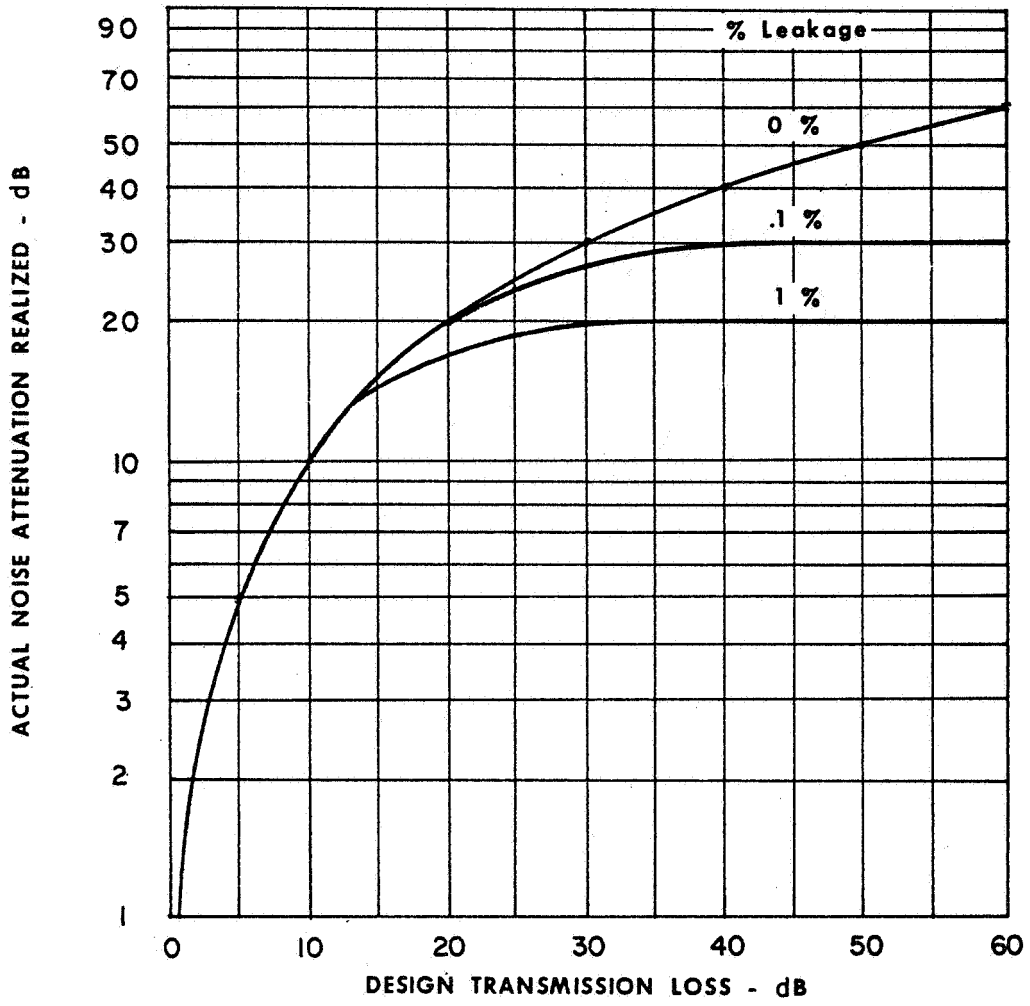

Figure 8.- Effect of leakage on panel transmission loss.

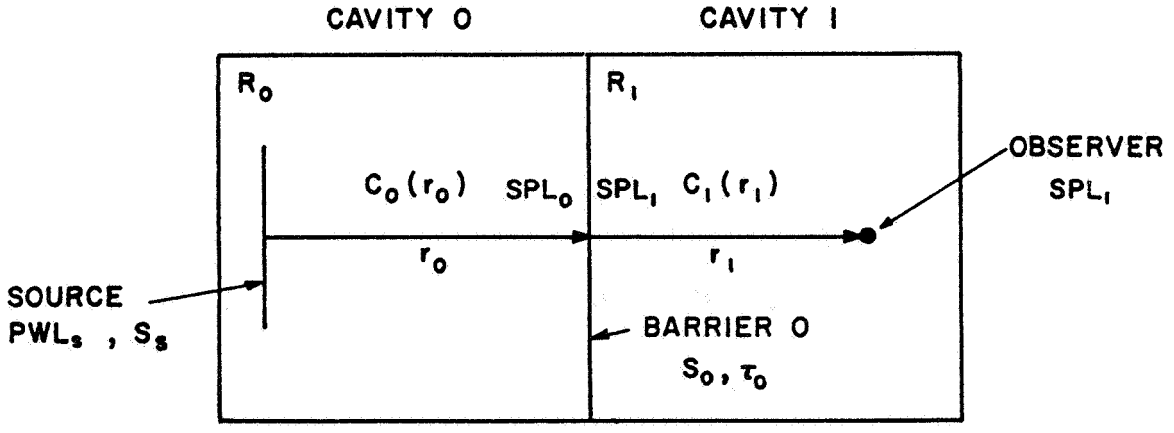

Figure 9.- Two-cavity problem.

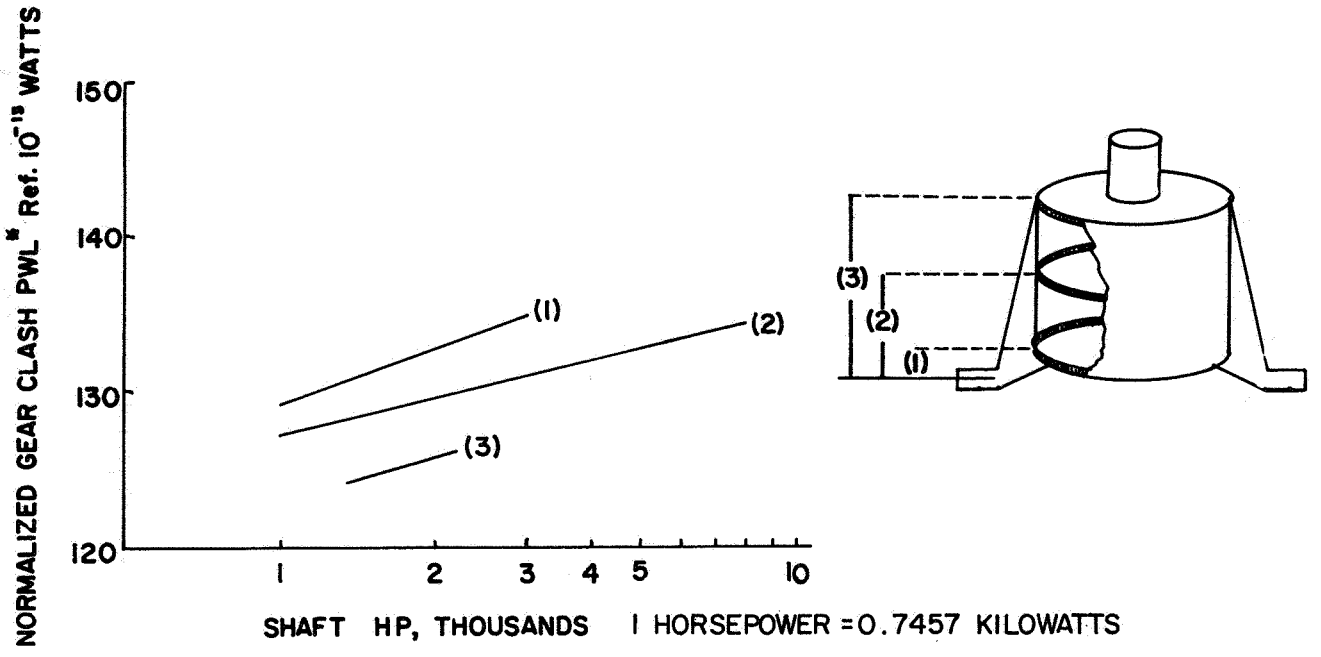

*LEVELS NORMALIZED TO PITCH LINE VELOCITY (plv) AND SPECIFIC TOOTH LOAD (stl) OF GEAR TRAIN IN CURVE (2)

$$\text{NORMALIZED PWL} = \text{PWL} - 20\,\text{LOG}(\text{plv}/\text{plv}_2) - 20\,\text{LOG}(\text{stl}/\text{stl}_2)$$

Figure 10. The effect of gearbox type on radiated PWL.

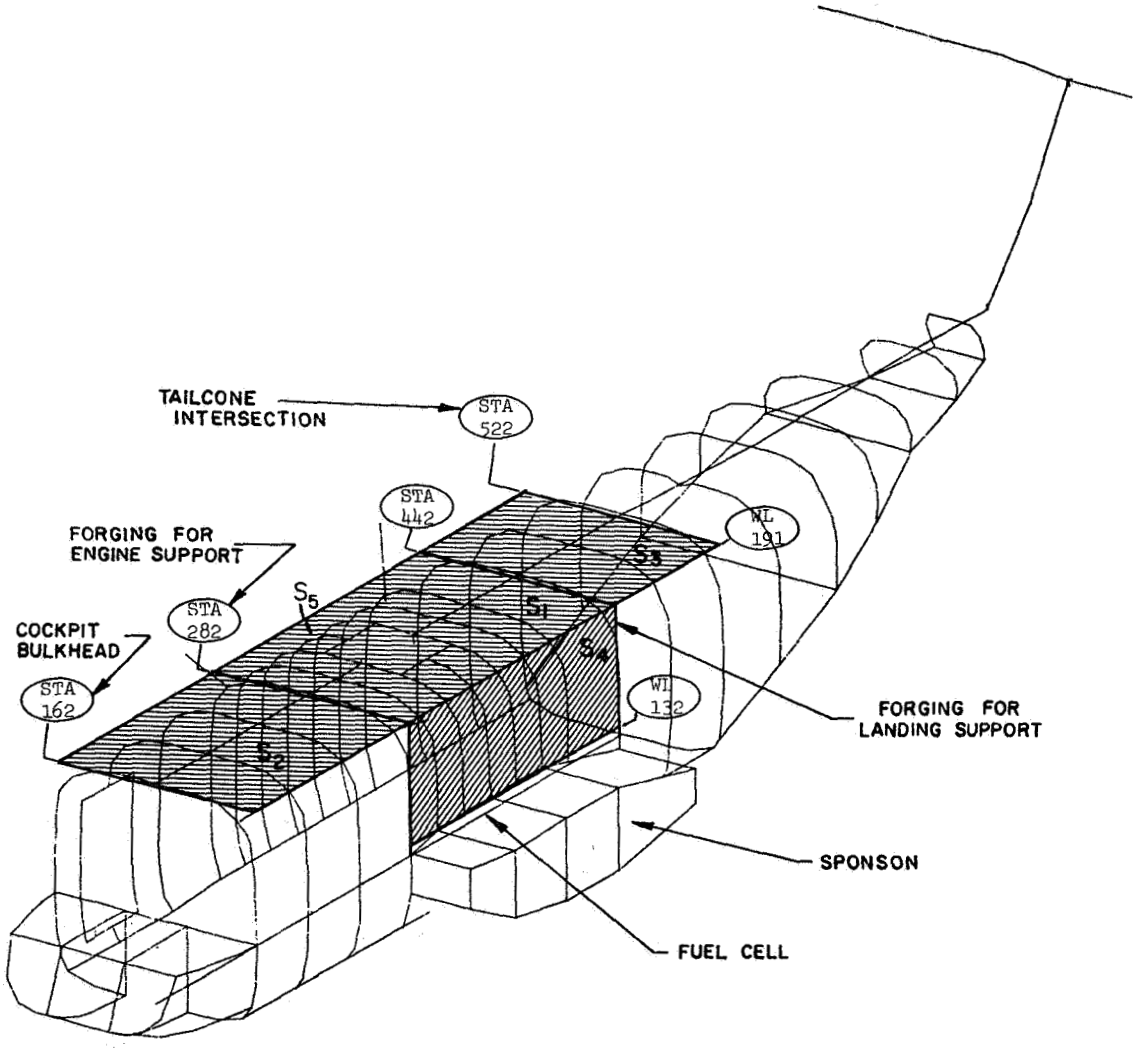

Figure 11.- Radiating surfaces for transmission noise based on the CHRA NASTRAN model.

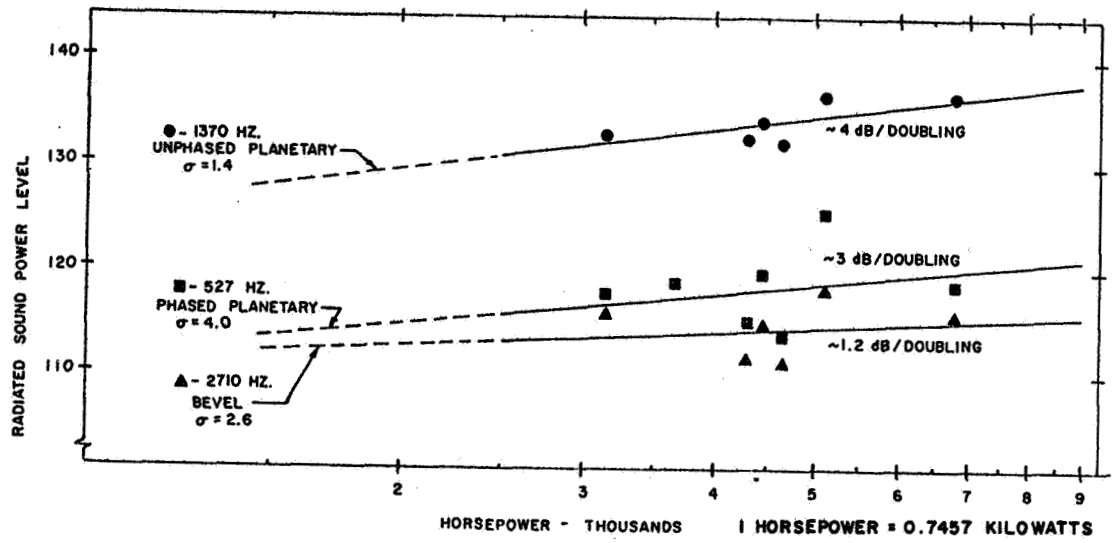

Figure 12.- Total radiated sound power levels versus consumed horsepower for CH-53 A/D aircraft.

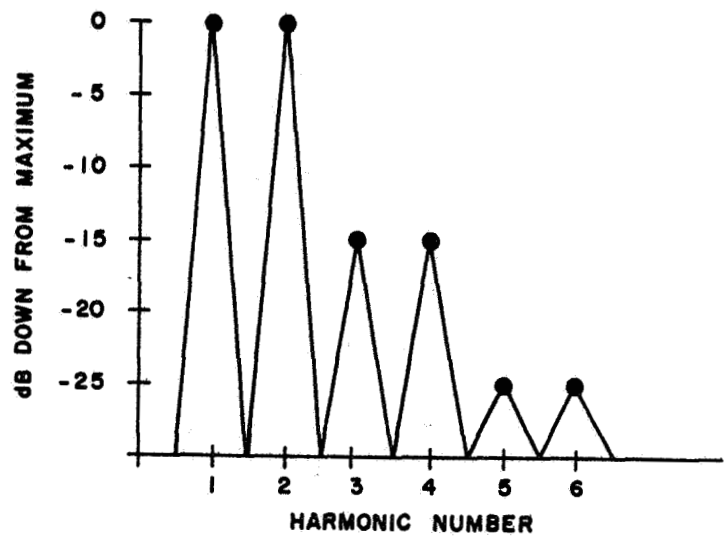

Figure 13.- Generalized gear noise harmonic spectrum.

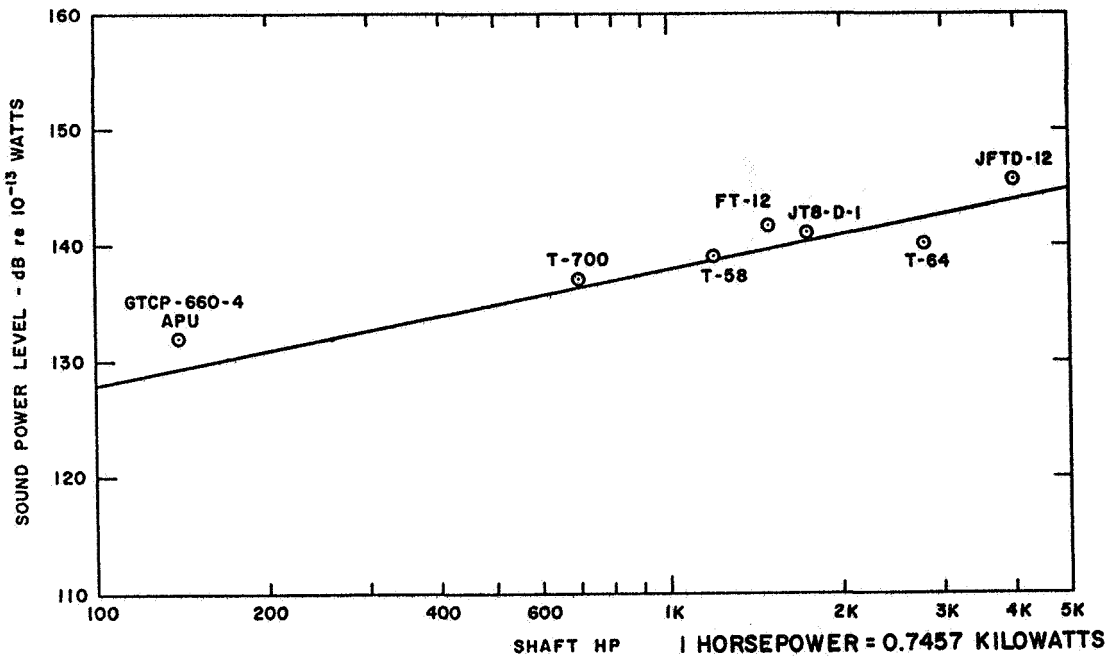

Figure 14.- Overall sound power level vs. horsepower for several engine types.

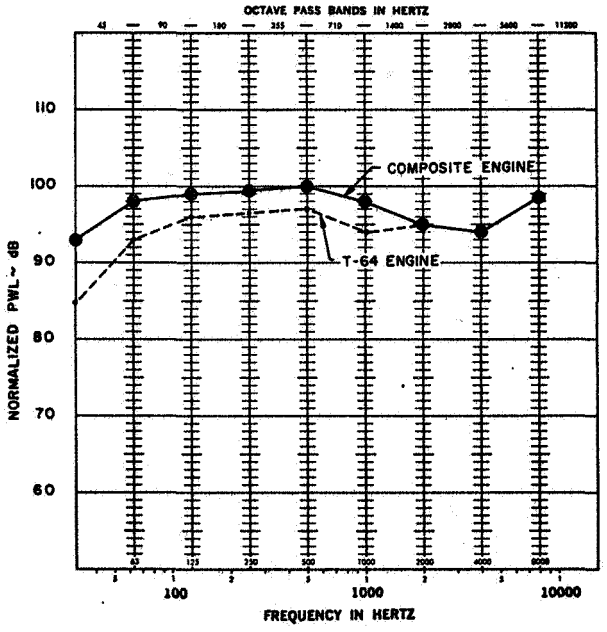

Figure 15.- Composite engine casing noise.

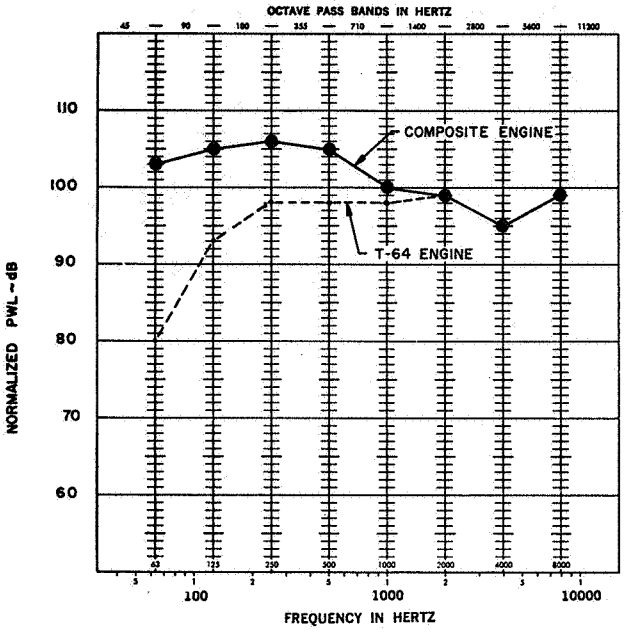

Figure 16.- Composite engine exhaust noise.

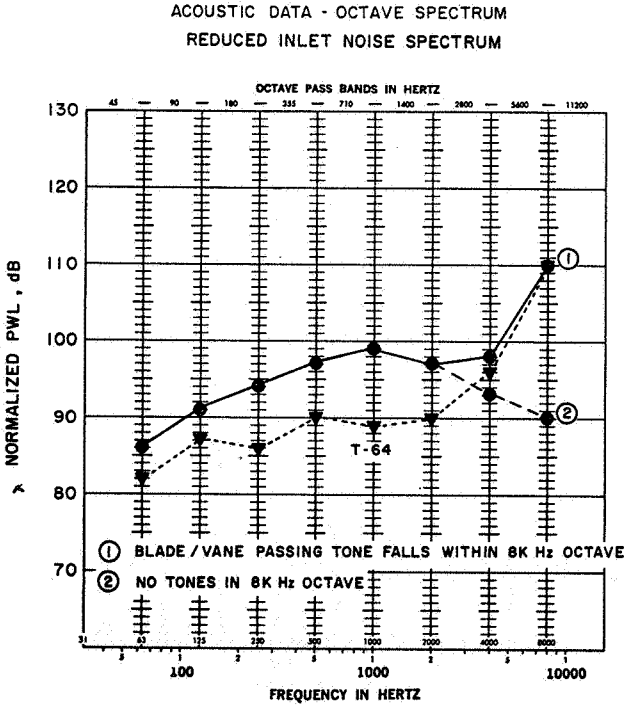

Figure 17.- Composite engine inlet noise.

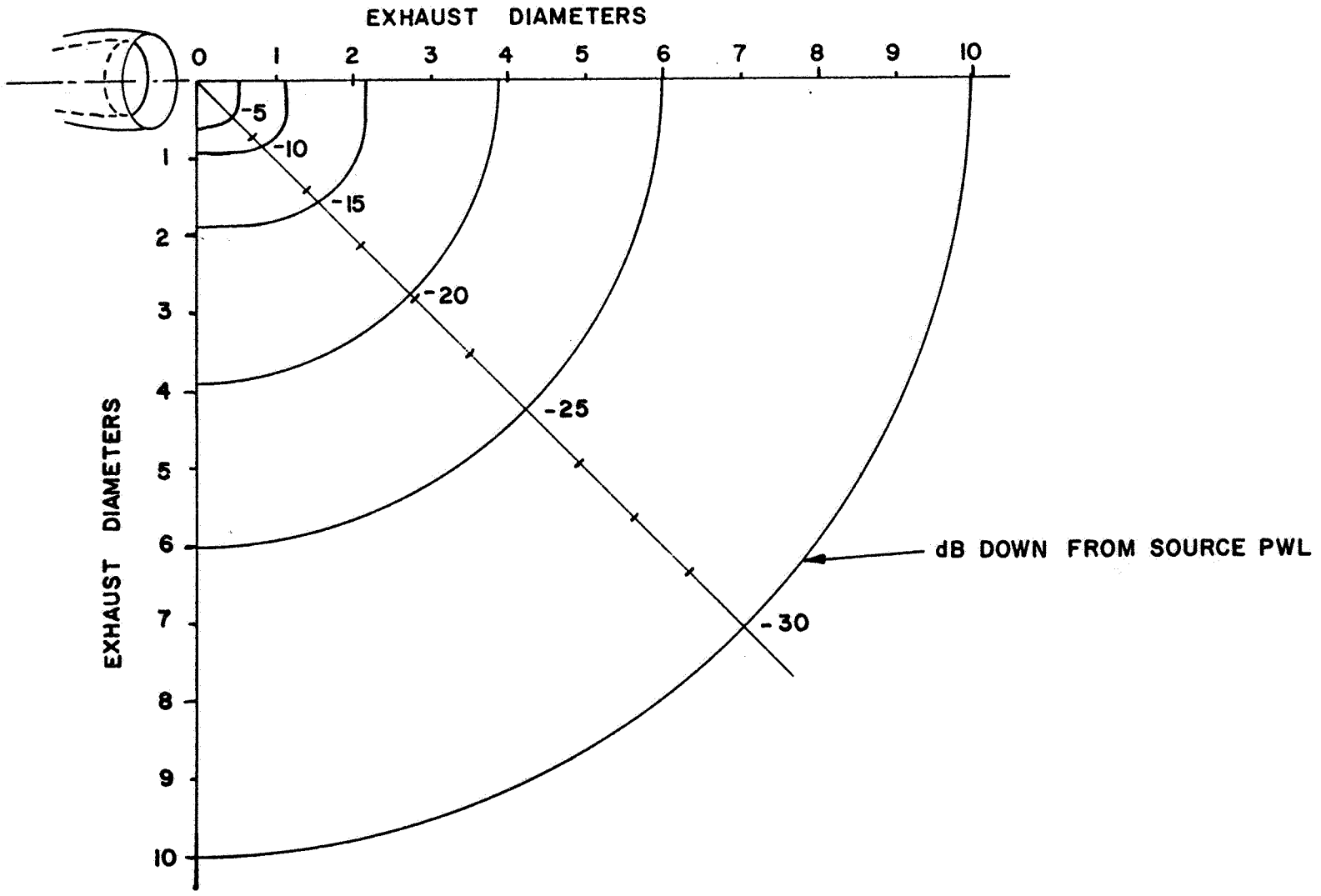

Figure 18.- Engine exhaust noise decay from source.

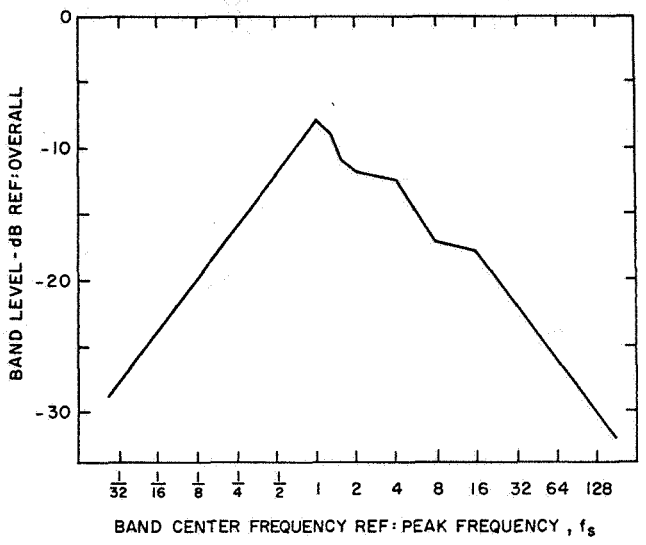

Figure 19.- Rotor broadband noise octave spectrum shape.

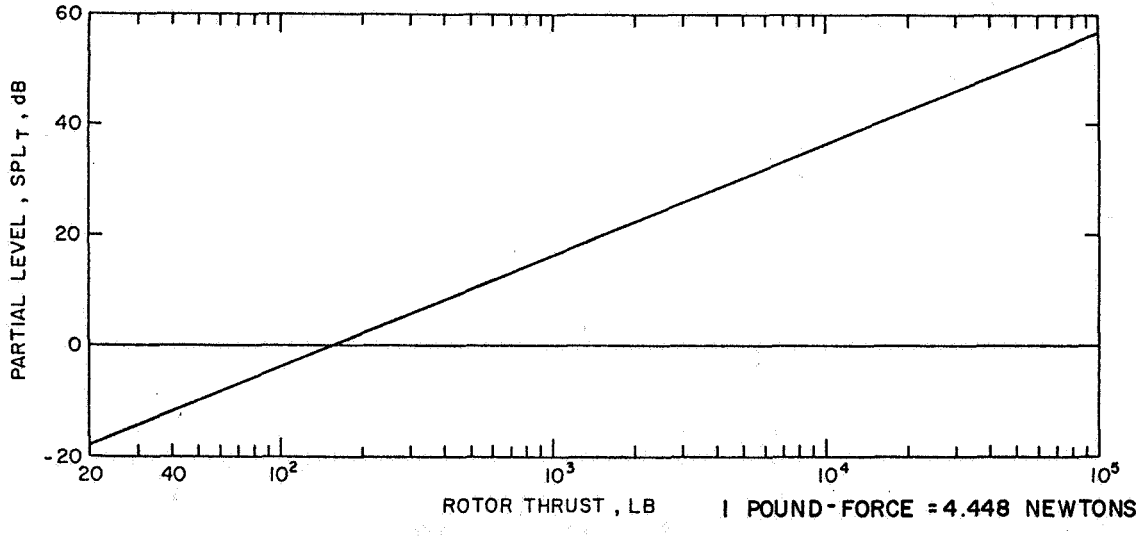

Figure 20.- Helicopter rotational noise partial level based on thrust.

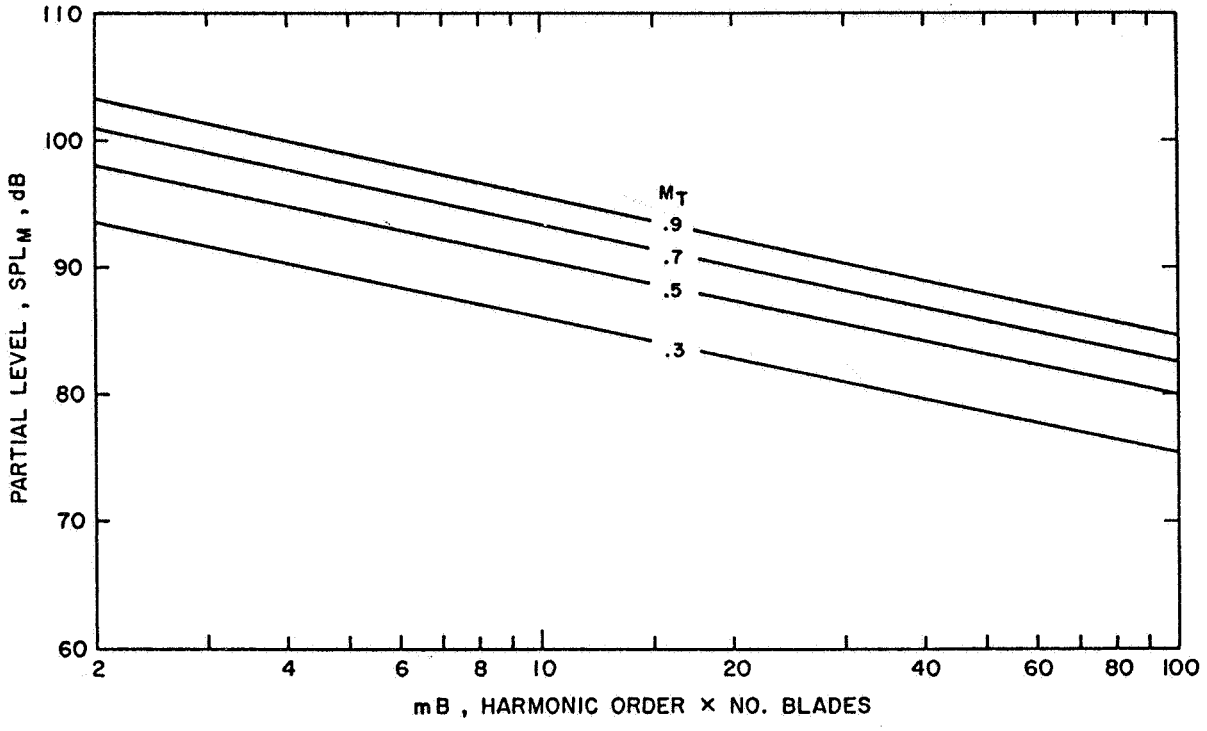

Figure 21.- On-axis thrust component SPL vs. harmonic order as a function of rotor tip Mach number M_T.

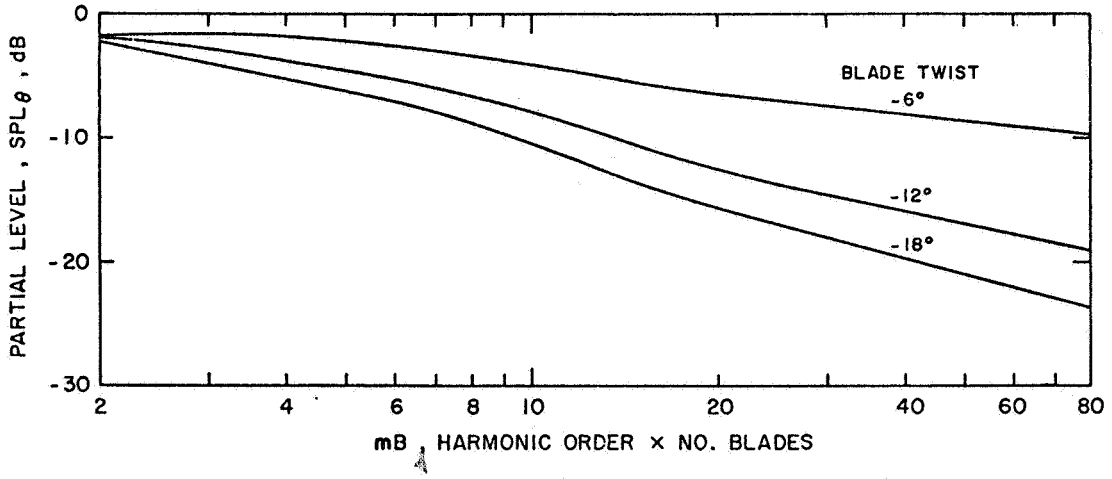

Figure 22.- Effect of twist on rotational noise harmonic thrust component.

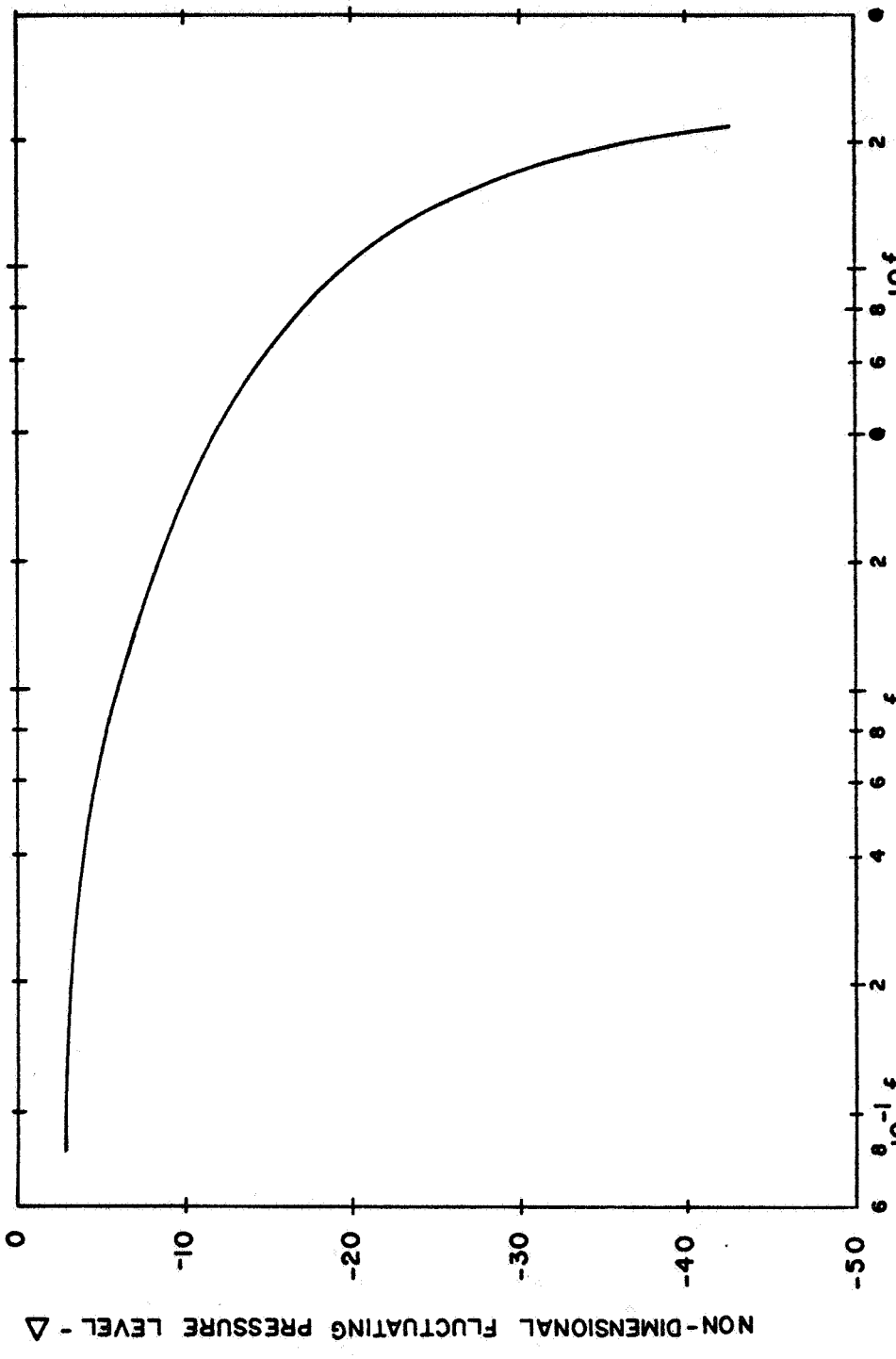

Figure 23.- Chart for estimating boundary layer pressure spectra.

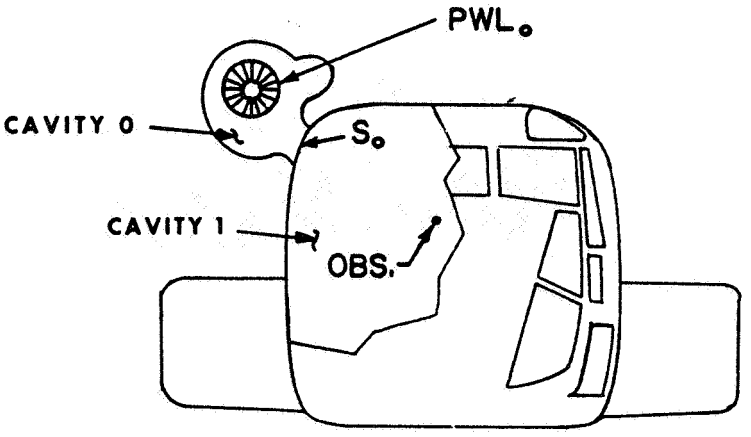

PHYSICAL PROBLEM

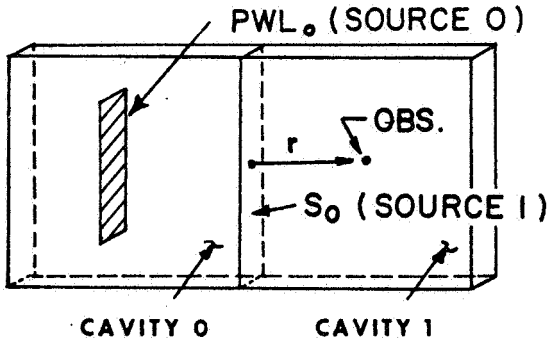

IDEALIZED PROBLEM

Figure 24.- Engine casing noise in bare cabin.

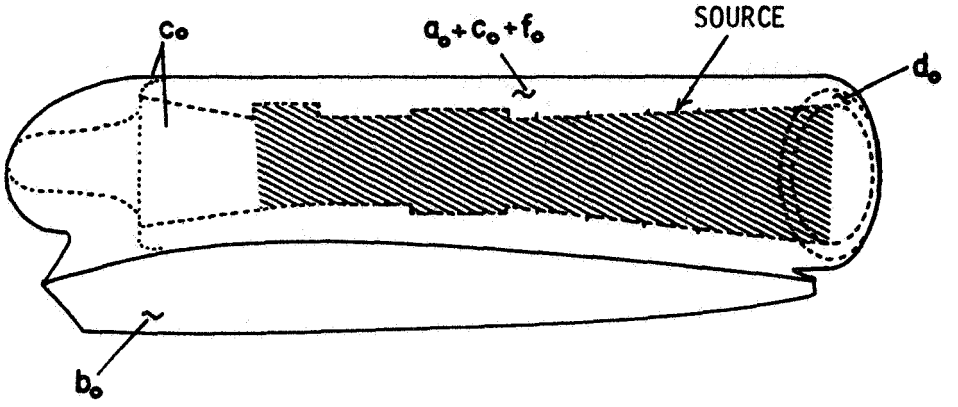

ENGINE/NACELLE ARRANGEMENT

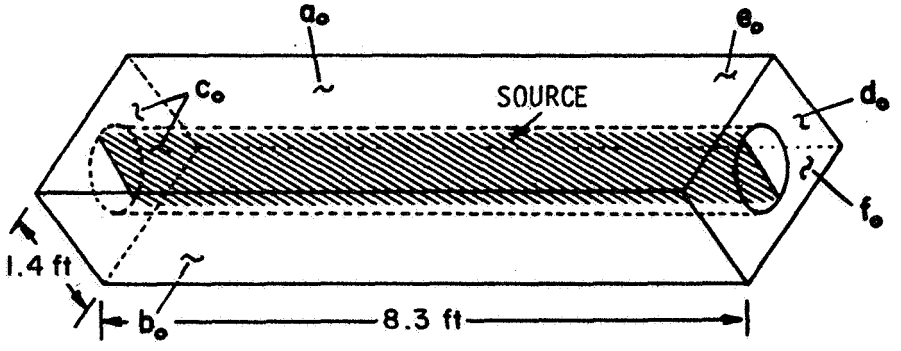

SIMPLIFIED ARRANGEMENT

Figure 25.- Source cavity representation.

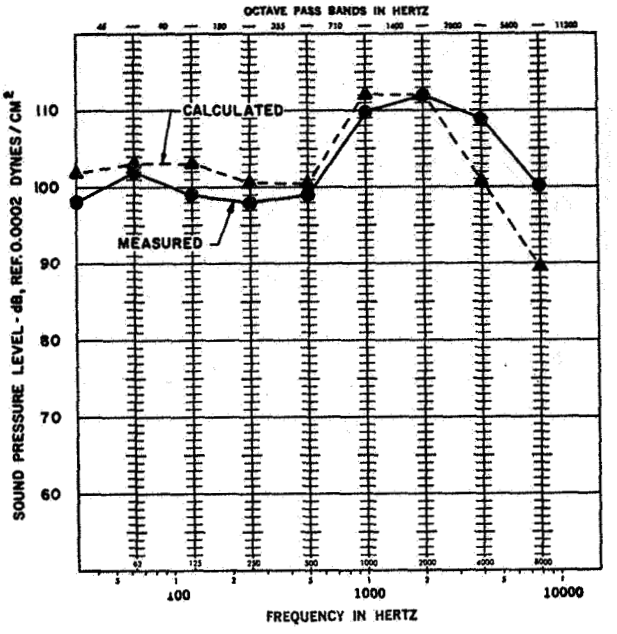

Figure 26.- Correlation of measured and predicted bare aircraft noise levels. Middle cabin; OGE hover.

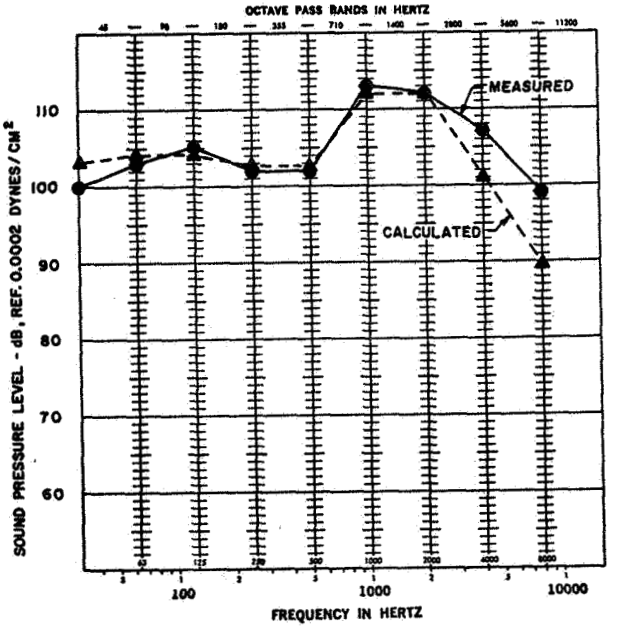

Figure 27.- Correlation of measured and predicted bare aircraft noise levels. Middle cabin; 150 knots indicated air speed.

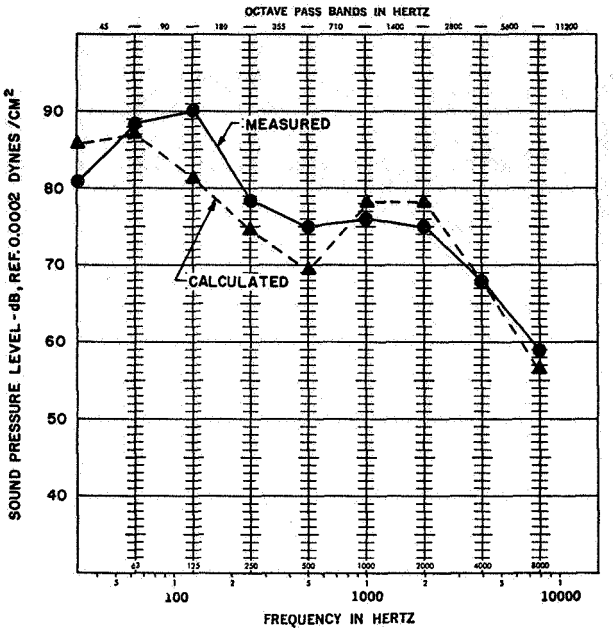

Figure 28.- Correlation of measured and predicted treated aircraft noise levels. Middle cabin; OGE hover.

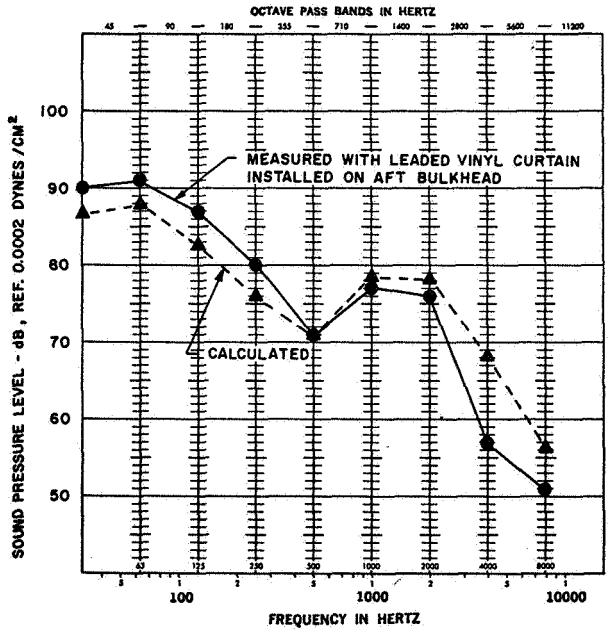

Figure 29.- Correlation of measured and predicted treated aircraft noise levels. Middle cabin; 150 knots indicated air speed.